Landau-Peierls instability, x-ray-diffraction patterns, and surface freezing in thin smectic films

Robert Holyst*
Department of Physics FM-15, University of Washington, Seattle, Washington 98195
(Received 15 March 1991; revised manuscript received 20 May 1991)

A model of x-ray diffraction for thin smectic-A liquid-crystal films is presented. The effect of the smectic-layer displacement fluctuations and correlations and the molecular form factor on the interlayer structure and the x-ray-diffraction pattern is discussed. In thin films the influence of the displacement-displacement correlation function on the x-ray-diffraction pattern is very small and can be neglected in the analysis of experimental data. On the other hand, both the displacement-fluctuation term (Debye-Waller factor) and molecular form factor produce strong measurable effects and so can be determined. We discuss the dependence of displacement fluctuations, calculated in the framework of the Landau–de Gennes model, on the smectic elastic constants and the smectic-vapor surface tension and show that these constants can be determined from the x-ray-diffraction pattern. The analysis of the hydrodynamic (collective) layer fluctuations and the individual molecular-motion fluctuations shows that the latter can be neglected in comparison to the former. The fluctuation amplitudes predicted by the model agree within 5% with the recent experimental measurements performed on smectic-I on -C films. In thin smectic films the fluctuation amplitudes $\sigma(\mathbf{r})=[\langle u^2(\mathbf{r})\rangle]^{1/2}$ are only ~ 4 Å compared with ~ 8 Å in a macroscopic sample. The fluctuations are suppressed at the two free surfaces by the large surface tension, grow away from each surface, and have a parabolic profile near the center of the film. We argue that one of the reasons for surface freeezing in smectic liquid crystals is the quench of the layer fluctuations by the large surface tension. However, we also show that in systems with small surface tension the fluctuations at the surface are in fact larger than the ones in the interior of the system. The growth of the diffuse scattering, due to the displacement-displacement correlations, with the thickness of the smectic film is discussed and shown to evolve towards the structure predicted for large samples by Gunther, Imry, and Lajzerowicz [Phys. Rev. A **20**, 1733 (1980)]. The model for the displacement layer fluctuations including the director as an independent variable is presented. Furthermore, the coupling between the layer fluctuations and the nematic order parameter in smectic liquid crystals is qualitatively discussed. It is argued that the compressional modes induce the nematic order-parameter fluctuations and that a large fluctuation profile may induce the smectic-A–smectic-C phase transition in thin films. Eventually in tilted smectic liquid crystals the layer fluctuation profile may induce a tilt profile. Finally, it is shown that the presented model can be applied to smectic systems other than smectic-A; we give explicit formulas for the x-ray-scattering intensity from the smectic-A_d films and also calculate the fluctuations amplitudes for the stratified smectic-I on -C system.

I. INTRODUCTION

Thin smectic films have been the subject of intensive experimental studies during the past decade [1–17]. The first optical experiments on extremely thin (≥ 50 Å, two and more layers thick) freely suspended ferroelectric smectic-C films were reported in 1978 in the seminal paper by Young *et al.* [1] and in 1979 by Rosenblatt *et al.* [2]. Inelastic light-scattering measurements were used in these papers to determine the dispersion relations for molecular orientation fluctuations [1] and to determine the average polarization, average tilt angle, Frank elastic constants, and viscosities as functions of the film thickness [2]. The success of these experiments proved that thin freely suspended smectic films are suitable systems for studying surface and finite-size effects. Since that time many different experiments using light scattering [1-5], electron diffraction [6], high-resolution ac calorimetry [7], and x-ray scattering [8–17] have been done on these systems. These experimental studies have been primarily aimed at the understanding of the phase transitions and thickness-dependent phase diagrams [3,7–11], the two-dimensional (2D)–3D evolution of the in-plane order and dimensional crossover [6,12–14], hexatic elastic constants in thin films and the dynamic of the hexatic order parameter [4,5], and surface freezing and wetting phenomena [15–17]. The theoretical studies have been mainly devoted to the phase transitions in 2D systems and the structure of 2D systems [18–24], and the evolution of the hexatic order between 2D and 3D systems [25,26]. Very recent experiments by Tweet *et al.* [27] and Gierlotka, Lambooy and de Jeu [28] demonstrated the utility of x-ray diffraction for studies of the interlayer structure of thin smectic films. Because the x-ray-diffraction pattern from thin films is much richer than the corresponding pattern from bulk samples, their interlayer structure can be studied in detail using diffraction. One of these experiments [27] has been performed on freely suspended films consisting of two hexatic smectic-I layers and interior smectic-C layers. The interlayer

structure of these films has been very well described by the Gaussian distribution for the layer positions with the Gaussian width given by the Landau–de Gennes theory for the displacement layer fluctuations in smectic-A films, adapted to include finite size and surface effects [29]. In addition, the smectic-I on -C films had a very distinct tilt profile induced by the smectic-I surface phase. The fits of the experimental data to the elastic theory for the tilt profile and the fluctuation profile allowed the determination of the smectic elastic constants, the surface tension, and the characteristic length for the decay of the tilt profile. The thin films have been shown to be more tilted and more ordered than thick ones [27]. Unfortunately, in the analysis of the experimental results the displacement-displacement correlation function has been completely neglected. Surprisingly, although this assumption is completely invalid for bulk samples [30], it has been shown to be a valid one for thin smectic films [31]. The aim of this paper is to give more details of the calculations not presented in Refs. [29,31] and also to present some new results for smectic-A_d, which should be applicable to the experiment on thin smectic-A_d films by Gierlotka, Labooy, and de Jeu [28]. Here we also present the complete expressions for the displacement-fluctuation profile for the stratified smectic-I on -C phase, studied experimentally by Tweet *et al.* [27], the evolution of the displacement-displacement smectic-A correlation function with the film thickness and discuss qualitatively the influence of the layer fluctuations on the surface freezing, smectic-A–smectic-C phase transitions in thin films, and the fluctuation-induced tilt profile in tilted smectic liquid crystals. We also discuss the saturation of the layer fluctuations in thin films and the influence of the very small surface tension on the fluctuation profiles. The paper is organized as follows: In Sec. II we recall the main results for large bulk samples; Sec. III is devoted to the discussion of fluctuations and correlations in thin films and their dependence on smectic elastic constants, surface tension, and the number of smectic layers; in Sec. IV the x-ray-diffraction pattern for thin smectic-A films is presented; in particular, we discuss there the effects of the finite size, the fluctuations, the correlations, and the molecular form factor on the x-ray-scattering intensity; finally, Sec. V is devoted to the discussion of the approximations made in the theory, the comparison to the experiment, the discussion of the director fluctuations, and the analysis of the hydrodynamic versus the molecular-motion fluctuations. Here we also discuss the concept of the x-ray correlation length and the relevance of the fluctuation profiles to the surface freezing in smectic liquid crystals and surface melting in simple fluids. Finally, we discuss the saturation of the layer fluctuations due to the finite-size effects and the influence of the small surface tension on the fluctuation profiles. The details of the calculations are relegated to the appendixes.

II. BULK SMECTIC-A SYSTEM

The smectic-A phase can be described as a one-dimensional stacking of equidistant two-dimensional liquid layers with the elongated liquid-crystal molecules perpendicular to the smectic layers (in our convention parallel to the z axis). Smectic-A liquid crystals are at lower marginal dimensionality and consequently, according to the Landau-Peierls argument [32], the layer fluctuation amplitudes diverge in the thermodynamic limit and destroy the long-range order. However, in practice, the logarithmic growth of the fluctuations with the size of the sample is so slow that it is very difficult to directly observe the destruction of the long-range smectic order in the typical experimental samples [33]. In order to estimate the amplitude of these fluctuations let us introduce the displacement perpendicular to the layers, $u_n(x,y)$, of the smectic layers from their equilibrium positions [34], $z=nd$. Here d is the layer spacing and n is the layer index. The free energy for the distortions of the smectic layer must be invariant with respect to any rotations of the system and also to the reflection with respect to the xy plane (z and $-z$ direction are equivalent). Assuming the continuous limit, $u_n(x,y)\rightarrow u(x,y,z)\equiv u(\mathbf{r})$, we find the following form of the bulk free energy [35]:

$$F_B=\tfrac{1}{2}\int d\mathbf{r}\left[B\left[\frac{du(\mathbf{r})}{dz}-\tfrac{1}{2}|\nabla u(\mathbf{r})|^2\right]^2+K[\Delta u(\mathbf{r})]^2\right]. \tag{2.1}$$

Here B is the smectic elastic constant associated with layer compressions and K is the elastic constant associated with layer undulations. One may easily check that the anharmonic terms in the bulk free energy are necessary to preserve the rotational invariance [35]. Although the effect of these terms on the renormalized B and K cannot be neglected in the infinite samples, nevertheless they can be neglected for typical experimental samples, because their influence there is rather small [35]. Dropping the anharmonic terms and neglecting the second derivative of u with respect to z in comparison to the first derivative, we find the bulk free energy in the harmonic approximation [30,34–36].

$$F_B=\tfrac{1}{2}\int d\mathbf{r}\left[B\left[\frac{du(\mathbf{r})}{dz}\right]^2+K[\Delta_\perp u(\mathbf{r})]^2\right]. \tag{2.2}$$

Here $\Delta_\perp$ is the Laplacian in x,y variables. If the system is large, but finite in the z direction and infinite in the two transverse directions, then the fluctuations far from the sample boundaries can be easily calculated using Eq. (2.2),

$$\sigma^2(\mathbf{r})\equiv\langle u^2(\mathbf{r})\rangle\approx\frac{k_BT}{4\pi\sqrt{KB}}\ln\frac{\sqrt{\lambda D_z}}{a_0}. \tag{2.3}$$

Here the statistical average $\langle\cdots\rangle$ is taken with respect to the $u(\mathbf{r})$, i.e.,

$$\langle\cdots\rangle=\int Du\cdots\exp\left[-\frac{F_B}{k_BT}\right], \tag{2.4}$$

D_z is the sample thickness, a_0 is the molecular diameter, k_BT is the Boltzmann factor, and $\lambda=\sqrt{K/B}$ is the characteristic smectic length in the system, which is of

the order of the layer spacing, d. For typical values of the parameters appearing in Eq. (2.2) (i.e., $\lambda=20$ Å, $D_z=1$ cm, $\sqrt{KB}=5$ dyn/cm, $a_0=4$ Å, and $k_BT=4\times10^{-14}$ erg), the corresponding layer fluctuations amplitude is $\sigma=7.7$ Å. Since these fluctuations are smaller than the layer spacing, $d=30$ Å, the smectic layers in a 1-cm-thick sample are still well defined. However, these 7.7-Å fluctuations dramatically reduce the intensity of the higher-order $(00l)$ reflections from the smectic layers [33,37]. For the system finite in the xy plane and infinite in the z direction we find, also using Eq. (2.2),

$$\sigma^2(\mathbf{r})\equiv\langle u^2(\mathbf{r})\rangle\approx\frac{k_BT}{4\pi\sqrt{KB}}\ln\frac{W}{a_0}\ , \tag{2.5}$$

where W is the linear dimension of the system in the xy plane. Assuming the same parameters as before and $W=1$ cm we find $\sigma=10.4$ Å.

As we have mentioned before, the layered structured of the smectic-A phase is destroyed in the thermodynamic limit due to the diverging fluctuations [see Eqs. (2.3) and (2.5)]. However, despite these divergent fluctuations smectic-A liquid crystals still possess quasi-long-range layer order even in the thermodynamic limit, because the interlayer density-density correlation function decays algebraically with the distance. This means that over large distances the layers fluctuate in unison. In addition, this slow algebraic decay of the correlation function leads to a strong diffuse scattering [30,36] (as opposed to the scattering from the perfectly ordered crystals). The interlayer scattering peak intensity $S(Q_z)$ diverges like

$$S(Q_z)=(Q_z-2\pi m/d)^{-2+\eta}\ , \tag{2.6}$$

where m is the index of the peak, d is the layer spacing, and Q_z is the momentum transfer in the z direction (we have confined our analysis to the interlayer structure only) and

$$\eta=Q_z^2\frac{k_BT}{8\pi\sqrt{KB}} \tag{2.7}$$

is the temperature and Q_z-dependent exponent [30,36]. Thus in the infinite smectic-A system the Bragg peaks characteristic for a one-dimensional solid are replaced by the power-law divergences. These predictions have been successfully checked in several experiments [33,38,39]. Of course, according to Eq. (2.6), there is only the finite number of peaks with diverging intensity; for large Q_z $\eta>2$, and instead of the divergence we have a cusp in the scattering intensity. One may estimate, using the aforementioned smectic parameters, that the fourth peak should be absent in the x-ray-diffraction pattern for an infinite sample.

For finite samples, there are two interesting limits: very thick and very thin. The very thick case has been treated by Gunther, Imry, and Lajzerowicz [36], who showed that the scattering pattern then consists of two parts, the aforementioned diffuse scattering plus a finite-size induced Bragg peak of width $\sim D_z^{-1}$ and height $\sim D_z W^{2-2\eta}$ on top of the diffuse scattering; here W is the finite sample size in the direction parallel to the layers and D_z is the sample size in the direction perpendicular to the smectic layers. The question we address in this paper is as follows: What happens in *thin* smectic samples?

III. THIN SMECTIC-A FILMS: FLUCTUATIONS AND CORRELATIONS

A. General formalism

We now consider a freely suspended thin smectic-A film with N_A layers [29,31]. The displacement fluctuations in this system are described by a free energy F with surface F_S and bulk F_B [Eq. (2.2)], contributions: $F=F_B+F_S$, with [29,31]

$$F_S=\tfrac{1}{2}\gamma\int d\mathbf{r}_\perp[|\nabla_\perp u(\mathbf{r}_\perp,z=0)|^2+|\nabla_\perp u(\mathbf{r}_\perp,z=Nd)|^2]\ . \tag{3.1}$$

This term describes the additional energy cost associated with increasing the surface area of the two free surfaces (located at $n=0$ and $n=N$). Here γ is a smectic-A vapor surface tension and $N_A=N+1$. Since the system consists of a finite number of layers in the z direction, it is natural to use a discrete version of this free energy with respect to z: $u(\mathbf{r}_\perp,z=nd)\equiv u_n(\mathbf{r}_\perp)$. Combining Eqs. (2.2) and (3.1) one easily finds [31]

$$F=\tfrac{1}{2}\int d\mathbf{r}_\perp\left[\sum_{n=0}^{N-1}\frac{B}{d}[u_{n+1}(\mathbf{r}_\perp)-u_n(\mathbf{r}_\perp)]^2+\sum_{n=0}^{N}Kd[\Delta_\perp u_n(\mathbf{r}_\perp)]^2+\gamma|\nabla_\perp u_0(\mathbf{r}_\perp)|^2+\gamma|\nabla_\perp u_N(\mathbf{r}_\perp)|^2\right]\ . \tag{3.2}$$

Now, taking the continuous Fourier transform with respect to $\mathbf{r}_\perp$ results in a compact expression for the free energy, F:

$$F=\tfrac{1}{2}\int d\mathbf{q}_\perp\sum_{k,n=0}^{N}u_k(\mathbf{q}_\perp)M_{kn}u_n(-\mathbf{q}_\perp)\ . \tag{3.3}$$

Here the only nonzero elements of the symmetric matrix $\underline{M}$ are on the diagonal and in the first off-diagonal positions. They are given by the following formulas:

$$M_{00}=M_{NN}=\gamma q_\perp^2+Kdq_\perp^4+\frac{B}{d}\equiv a\ , \tag{3.4}$$

$$M_{nn}=Kdq_\perp^4+\frac{2B}{d}\equiv b,\quad n=1,\ldots,N-1 \tag{3.5}$$

$$M_{n+1n}=M_{nn+1}=-\frac{B}{d}\equiv c\ ,\quad n=0,\ldots,N-1\ . \tag{3.6}$$

The layer displacement fluctuations $\langle u_n^2(\mathbf{r}_\perp)\rangle$ and the displacement correlation function $\langle u_k(\mathbf{r}_\perp)u_n(0)\rangle$ can now be calculated using the elements of $\underline{M}^{-1}$, namely,

$$\sigma_n^2(\mathbf{r}_\perp)=\langle u_n^2(\mathbf{r}_\perp)\rangle=k_BT\frac{1}{(2\pi)^2}\int d\mathbf{q}_\perp(\underline{M}^{-1})_{nn} \tag{3.7}$$

and

$$\langle u_k(\mathbf{r}_\perp)u_n(0)\rangle=k_BT\frac{1}{(2\pi)^2}\int d\mathbf{q}_\perp(\underline{M}^{-1})_{kn}\exp(i\mathbf{q}_\perp\cdot\mathbf{r}_\perp)\ . \tag{3.8}$$

The limits of these integrations are $2\pi/W < |q_\perp| < 2\pi/a_0$; the lower limit is set by the transverse size of the film, W, and the upper limit is set by the molecular diameter since transverse modes with wavelengths smaller than the molecular diameter or larger than the film cannot be excited. For real measurements, the long-wavelength cutoff will usually be set by the instrument resolution (or, in other words, by the photon correlation length) rather than by the sample size [27]. This point will be discussed further in Sec. V. The elements of the matrix $\underline{M}^{-1}$ are given by

$$(\underline{M}^{-1})_{kn} = (-1)^{n+k} \frac{A_k c^{|n-k|} A_{N-n}}{C_{N+1}} , \tag{3.9}$$

for $n \geq k$ (otherwise n and k should be exchanged). Here

$$C_n = a^2 T_{n-2} - 2ac^2 T_{n-3} + c^4 T_{n-4} , \quad n > 2 \tag{3.10}$$

$$A_n = aT_{n-1} - c^2 T_{n-2}, \quad n = 1, \ldots, N \tag{3.11}$$

$$T_n = b^n \frac{\eta_+^{n+1} - \eta_-^{n+1}}{\eta_+ - \eta_-} , \tag{3.12}$$

and

$$\eta_\pm = \frac{1 \pm [1 - 4(c/b)^2]^{1/2}}{2} . \tag{3.13}$$

For $n = 0$, $A_n = 1$. The inversion of the matrix $\underline{M}$, although standard [40], is presented for completeness in Appendix A.

B. Displacement fluctuations

First of all we will present the results of the calculations for the displacement fluctuations given by Eq. (3.7). Most of the calculations were performed assuming typical smectic parameters: $K = 10^{-6}$ dyn and $B = 2.5 \times 10^7$ dyn/cm^2 (so $\lambda = 20$ Å), $d = 30$ Å, $a_0 = 4$ Å, $\gamma = 30$ dyn/cm, and $W = 4 \times 10^4$ Å (W is estimated in Sec. V). The calculated fluctuation profile $\langle u_n^2(\mathbf{r}_\perp) \rangle$ versus the layer index n for 5, 11, 35, and 61 layers and for different values of the surface tension is presented in Fig. 1. For visual clarity the layer index n runs between $-N/2$ and $+N/2$ in all the figures (instead of 0 and N as the formulas presented in the preceding section). For later convenience all the figures present the fluctuation amplitude squared; nonetheless, in the discussion of the figures we will also give values of the fluctuation amplitudes. The fluctuation amplitudes $\sigma_n = (\langle u_n^2 \rangle)^{1/2}$ at the surface are suppressed by $\sim 1-2$ Å relative to the fluctuations inside the sample and grow rapidly in the first few layers close to the surface. For thicker films (e.g., 35 layers) the fluctuation amplitudes have a parabolic profile in the center of the film. The maximum amplitude occurs at the center of the film and the center fluctuations grow from ~ 3 Å for a 3-layer thick film to ~ 4.7 Å for a 61-layer thick film. At the surface the layer fluctuations are strongly suppressed by the surface tension and only weakly depend on the film thickness. For infinitely thick films with the transverse cutoff, $W = 4 \times 10^4$ Å, the layer fluctuation amplitude at the center of the film σ_C, estimated from Eq. (2.5), is 7.6 Å. At the same time the surface fluctuation amplitude σ_S is $\sim 3-4$ Å, because as we can see from Fig. 1 the surface fluctuations hardly depend on the film thickness. The difference between the surface and the bulk fluctuations induces, far from the surface, a slowly varying parabolic profile for the fluctuation amplitudes. In Figs. 1(b) and Fig. 1(c) the profiles are presented for $\gamma = 5$ dyn/cm and 100 dyn/cm to be compared

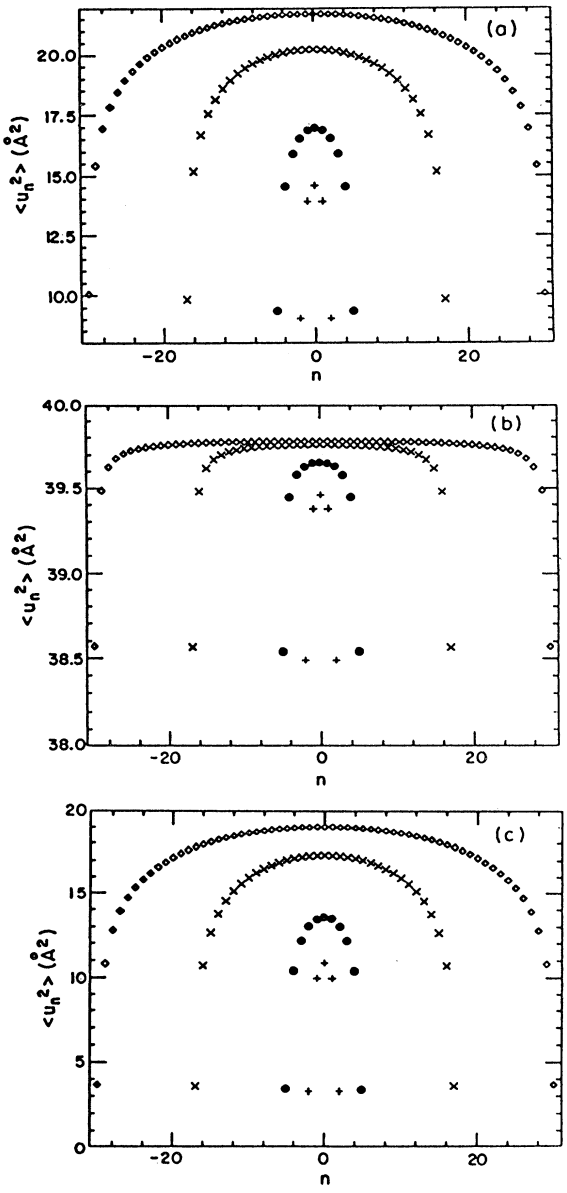

FIG. 1. The discrete layer displacement fluctuation profile $\sigma_n^2 = \langle u_n^2 \rangle$ vs the index layer n for a 5-layer-thick film (+), an 11-layer-thick film (●), a 35-layer-thick film (×) and a 61-layer-thick film (◇). For visual clarity the layer index runs from $-N/2$ to $N/2$, where $N+1$ is the number of layers. Here $n = 0$ corresponds to the center of the film and $n = -N/2$ and $N/2$ corresponds to two free surfaces. $B = 2.5 \times 10^7$ dyn/cm^2 and $K = 10^{-6}$ dyn are smectic elastic constants and γ is the smectic/vapor surface tension; (a) $\gamma = 30$ dyn/cm, (b) $\gamma = 5$ dyn/cm, (c) $\gamma = 100$ dyn/cm.

with Fig. 1(a) for $\gamma=30$ dyn/cm. From Fig. 1(b) (small γ) we see that the fluctuation profile is very weak (the difference between the surface fluctuations and the center ones is very small). Moreover, the profile is very flat in the center of the film and the value of σ_C as well as σ_S hardly changes with the film thickness. Large surface tension [Fig. 1(c)] strongly affects fluctuations at the surface but not the fluctuations in the center.

The dependence of the profiles for 5-, 11-, 35-, and 61-layer thick films on the smectic elastic constants, B and K is shown in Fig. 2. In Figs. 2(a) and 2(b) the profiles are shown for $B=25\times10^7$ and 0.25×10^7 dyn/cm^2, respectively, to be compared to Fig. 1(a) for $B=2.5\times10^7$ dyn/cm^2 (in all three cases $\gamma=30$ dyn/cm and $K=10^{-6}$ dyn). As one can see, the surface fluctuations hardly depend on B, whereas the interior fluctuations are very strongly affected. Large B [Fig. 2(a)] flattens the profile in the films, whereas small B [Fig. 2(b)] makes the profile more pronounced. The same observations hold also if K is changed instead of B [see Figs. 2(c) and 2(d)]. It is clear that increasing either B or K suppresses fluctuations throughout the sample and that this suppression is much stronger inside the sample than at the surface. It is also clear from Fig. 2 that, as expected from Eqs. (2.3) and (2.5) the fluctuation amplitudes are more sensitive to $\beta=\sqrt{KB}$ than they are to $\lambda=\sqrt{K/B}$. B and K do not change the surface fluctuations very much because $\gamma\gg\sqrt{KB}$.

The calculated dependence of $\sigma_S^2=\langle u_{-N/2}^2\rangle=\langle u_{N/2}^2\rangle$ and $\sigma_C^2=\langle u_0^2\rangle$ on the smectic-A-vapor surface tension and the smectic elastic constant B is shown in Fig. 3. First we discuss their dependence on γ. The asymptotic dependence of σ_S and σ_C on γ follows directly from Eqs. (3.4)–(3.13): for very large values of the surface tension σ_S approaches zero as $\sim\gamma^{-1}$; for very small surface tension both σ_S and σ_C diverge as $\sim q_\perp^{-2}$ up to the limit set by the transverse cutoff $q_\perp=2\pi/W$. Here we note that for the very small surface tension ($\gamma\ll\sqrt{KB}$) we find that $\sigma_S>\sigma_C$. This point will be analyzed further in the discussion. Below we will only consider the case of $\gamma\geq\sqrt{KB}$. Both σ_S and σ_C decrease with increasing γ [Figs. 3(a) and 3(b)]. However, the surface amplitude σ_S approaches zero as γ increases while the center amplitude approaches a finite nonzero value, which only depends on the thickness of the film and the smectic elastic

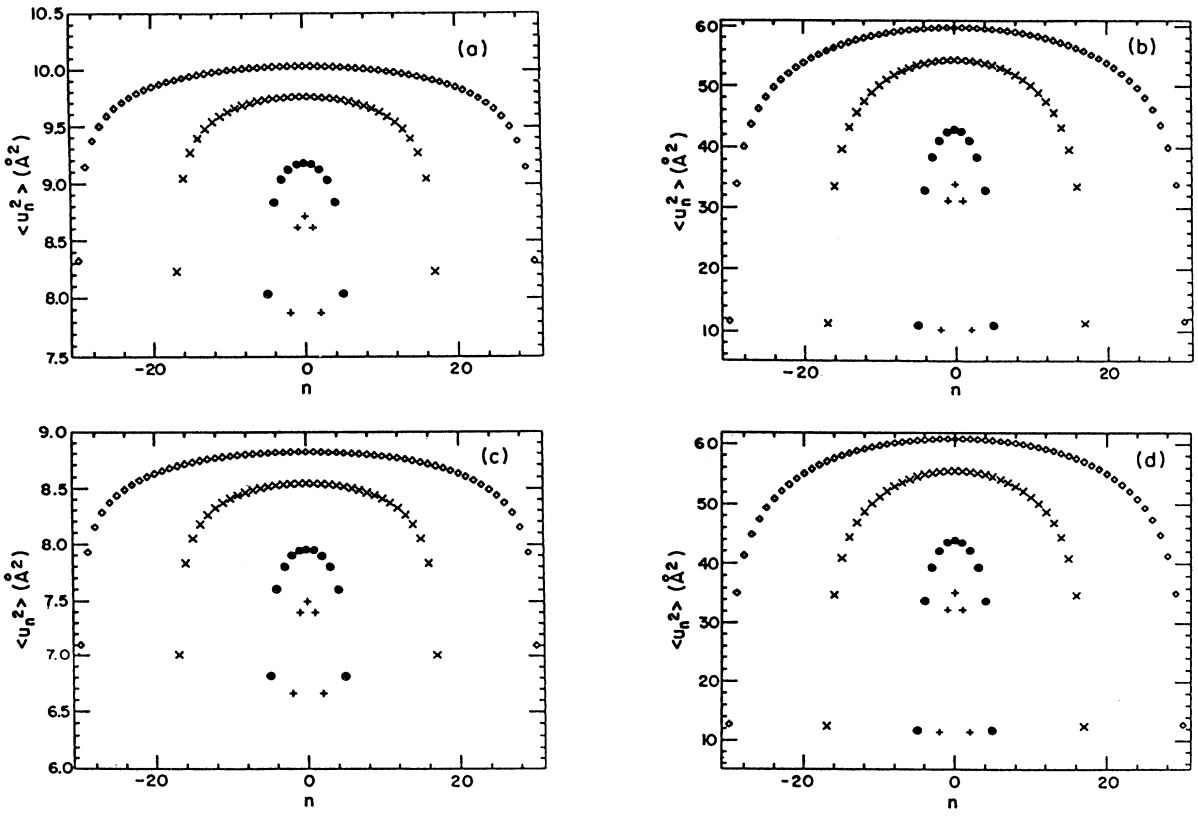

FIG. 2. Fluctuation profile vs the layer index n for different smectic elastic constants B and K. Legend as in Fig. 1(a); (a) $K=10^{-6}$, $B=25\times10^7$ dyn/cm^2; (b) $K=10^{-6}$, $B=0.25\times10^7$ dyn/cm^2; (c) $K=10^{-5}$, $B=2.5\times10^7$ dyn/cm^2; (d) $K=10^{-7}$, $B=2.5\times10^7$ dyn/cm^2.

constants. Thus for large γ the surface amplitude is much more affected than the center amplitude. Moreover, the surface amplitude hardly depends on the film thickness for any value of γ, whereas the center amplitude strongly depends on the layer thickness for large γ but only weakly for small γ (see Fig. 3). For very small surface tension the values of the fluctuation amplitudes for the whole profile are dominated by the presence of the surface. On the other hand, for large γ only the surface amplitude strongly depends on the surface tension. The dependence of σ_S^2 on B is shown in Fig. 3(c) and the dependence of σ_C^2 on B is shown in Fig. 3(d). For very small B the interior fluctuations strongly grow, whereas the surface fluctuations hardly change, being dominated in the first place by the surface tension. For very thin films it leads to large fluctuation gradients. This means that in the limit of small B and K, the presented model is no longer valid and other effects like the anharmonic terms, director fluctuations and the quasi-"surface terms" for the inside layers have to be included. All these effects are mentioned in the discussion.

C. Displacement-displacement correlation function

The displacement-displacement correlation function $\langle u_k(\mathbf{r}_\perp)u_n(0)\rangle$ provides information about the typical wavelength of the layer fluctuations. This function can be positive or negative; a positive value of the correlation function means in this case that different layers fluctuate in unison; negative values mean the opposite. The case $\mathbf{r}_\perp=0$ provides information about the compressional modes. In addition, studying $\langle u_k(\mathbf{r}_\perp)u_k(0)\rangle$ for different k and $\mathbf{r}_\perp$ gives information about the undulational modes.

The displacement correlations $\langle u_k(0)u_n(0)\rangle$ (for $\mathbf{r}_\perp=0$) as functions of n for a 61-layer thick film is presented in Fig. 4(a) for $k=0, -10, -20, -30$. Here $k=0$ corresponds to the center layer, whereas $k=-30$ corresponds to the surface layer. As can be seen from this figure all the layers in the thin films are very strongly correlated; even the two surface layers separated by $(N+1)d=1800$ Å ($d=30$ Å) are fluctuating in unison. In the case of $k=-30$ the correlation function changes from 10 Å^2 for $n=-30$ to 3 Å^2 for $n=30$. For com-

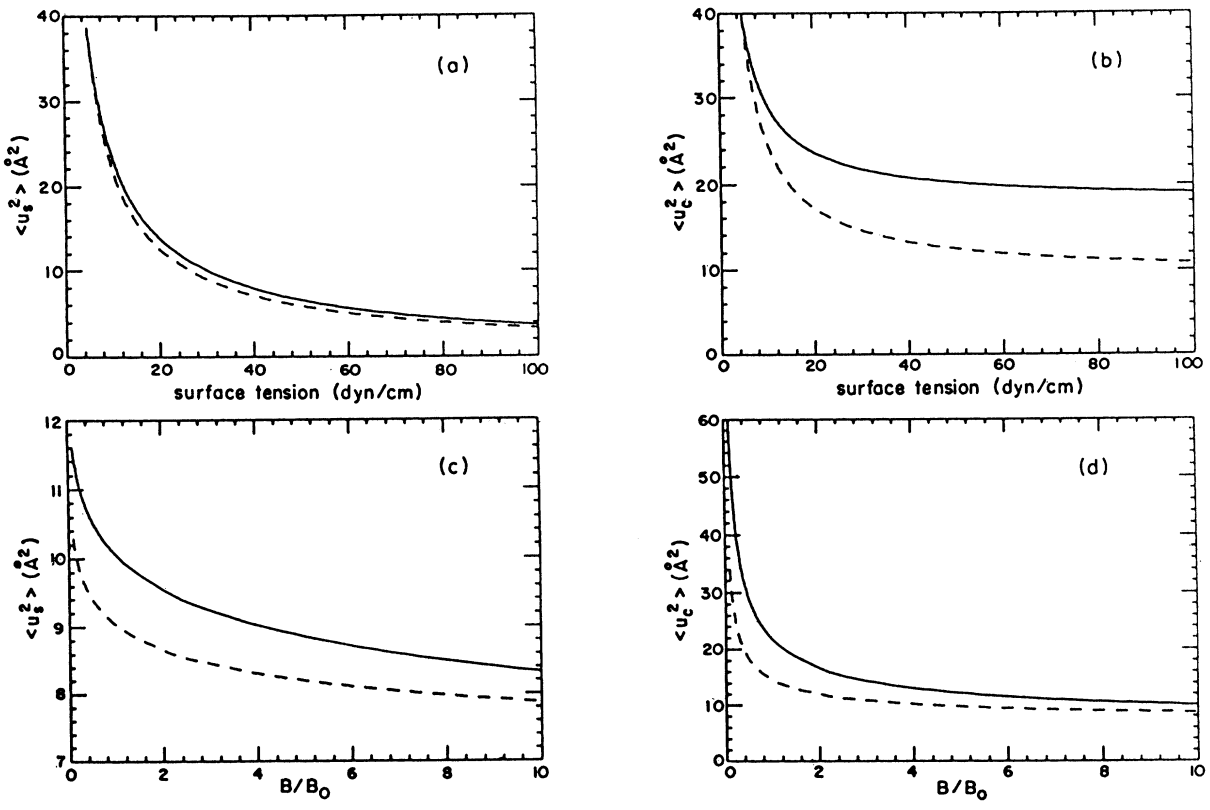

FIG. 3. The surface fluctuations, $\langle u_S^2\rangle=\langle u_{-N/2}^2\rangle=\langle u_{N/2}^2\rangle$ [cases (a) and (c)] and the fluctuations in the center of the film $\langle u_C^2\rangle=\langle u_0^2\rangle$ [cases (b) and (d)] vs the smectic vapor surface tension, γ [cases (a) and (b)] and the smectic elastic constant B [cases (c) and (d)] for a 5-layer-thick film (dashed line) and a 61-layer-thick film (solid line) $N+1$ is the film thickness. (a) and (b) $B=2.5\times10^7$ dyn/cm^2, $K=10^{-6}$ dyn; (c) and (d), $B_0=2.5\times10^7$ dyn/cm^2, $K=10^{-6}$ dyn, $\gamma=30$ dyn/cm.

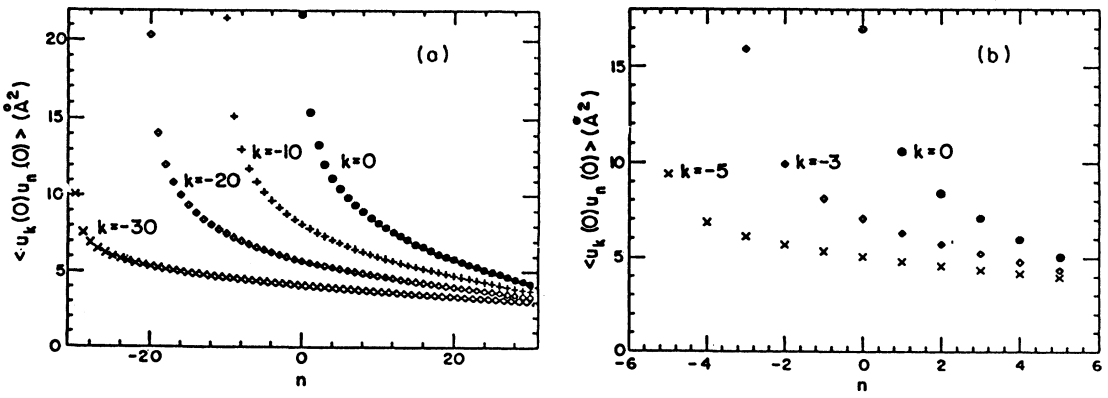

FIG. 4. The correlation function $\langle u_k(0)u_n(0)\rangle$ vs the layer index n for $B=2.5\times10^7$ dyn/cm^2, $K=10^{-6}$ dyn, $\gamma=30$ dyn/cm and (a) a 61-layer-thick film for $k=0$ (●), $k=-10$ (+), $k=-20$(◇), and $k=-30$(×). Here $k=0$ corresponds to the center layer of the film, whereas $k=-30$ corresponds to one of the surface layers; (b) an 11-layer-thick film for $k=0$ (●), $k=-3$(◇), and $k=-5$(×). Here $k=0$ corresponds to the center of the film and $k=-5$ corresponds to one of the surface layers.

parison we show in Fig. 4(b) the correlation function for the 11-layer-thick film for $k=0,-3,-5$; here $k=0$ corresponds to the center layer and $k=-5$ corresponds to the surface layer. The behavior of the correlation function in this case is very similar to the previous one.

The displacement correlation function $\langle u_k(\mathbf{r}_\perp)u_n(0)\rangle$ for fixed k and n as a function of $r_\perp=|\mathbf{r}_\perp|$ is shown in Fig. 5(a). The correlation function is positive for $r_\perp\leq1000a_0$ ($a_0=4$ Å); for larger $r_\perp$ it starts to oscillate around zero with the typical amplitude much smaller than 1, which slowly goes to zero. So the typical wavelength of the undulations in our finite system ($W=40\,000$ Å) is ~4000 Å and thus can be probed also with light scattering. Of course for the infinite sample size ($W=\infty$) this wavelength is also infinite. One also observes that the correlation function for different (k,n) pairs tends to the same limit for large $r_\perp$ and practically for $r_\perp$ greater than $100a_0$ it has the same values regardless of (k,n). For comparison a similar figure for an 11-layer-thick film is shown in Fig. 5(b).

In the next section the influence of the fluctuations and correlations, calculated in this section, on the x-ray-scattering intensity, $S(Q_z)$, is presented.

IV. X-RAY-DIFFRACTION PATTERNS FOR THIN SMECTIC-A FILMS

The interlayer structure information is reflected in the x-ray-diffraction intensity, $S(Q_z)$, which is the Fourier transform of the density-density correlation function,

$$S(Q_z)=\int d\mathbf{r}\int d\mathbf{r}'\langle\hat{\rho}(\mathbf{r})\hat{\rho}(\mathbf{r}')\rangle\exp[iQ_z(z-z')]\,. \tag{4.1}$$

We assume that the multiple scattering and attenuation of the incident beam in the sample can be neglected. In general, the x-ray multiple scattering can be neglected be-

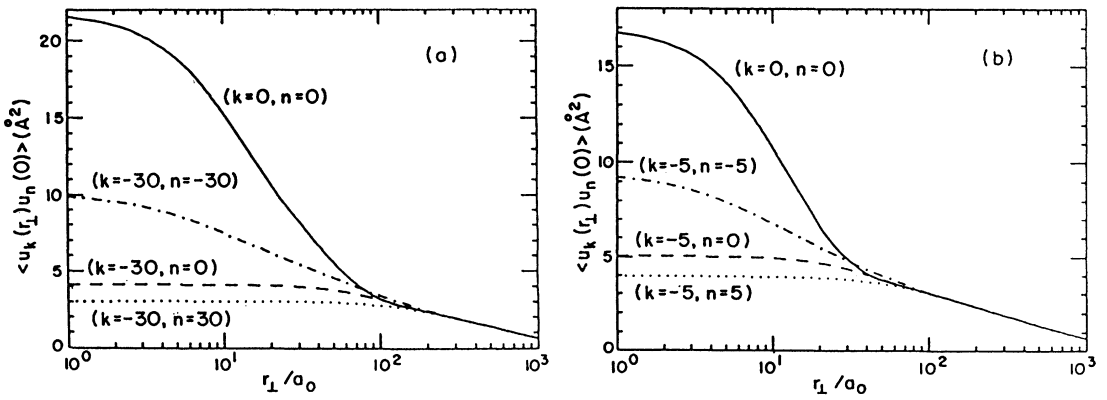

FIG. 5. The correlation function $\langle u_k(r_\perp)u_n(0)\rangle$ vs the in-plane distance $r_\perp$ for different layer indices, n and k, and for two different numbers of layers; 61 [case (a)] and 11 [case (b)]. Here $a_0=4$ Å is the molecular diameter, $B=2.5\times10^7$ dyn/cm^2, $K=10^{-6}$ dyn and $\gamma=30$ dyn/cm. $k=0$, $n=0$ (solid line) corresponds to the center layer, $k=-30$ and $n=-30$ [case (a)] and $k=-5$ and $n=-5$ [case (b)] corresponds to the surface layer (dash-dotted line).

cause the Thompson cross section for electron-photon scattering is very small $[(e^2/mc^2)^2 \simeq 10^{-10}$ Å$^2)]$ [41]. In thin films practically all of the incident beam is passing through the sample, thus the last effect can also be safely ignored. In thin smectic films the density operator $\hat{\rho}$ can be written in the following form:

$$\hat{\rho}(\mathbf{r}) = \rho_s \sum_{n=0}^{N} \int dz' \delta(z - z' - nd - u_n(\mathbf{r}_\perp)) \rho_M(z') \ . \tag{4.2}$$

Here ρ_s is the number of molecules per unit surface area of the layer and ρ_M is the molecular electron density along the z direction (i.e., the electron density of the liquid-crystal molecule projected onto the z axis). The δ function $\delta(z - nd - u_n)$ specifies the location of the nth layer in space in terms of the displacement u_n of the nth layer from its equilibrium position $z = nd$. The statistical average $\langle\ \rangle$ is taken with respect to the u_n [see Eq. (2.4)] with the free energy given by Eq. (3.2). By combining Eqs. (4.1) and (4.2) $S(Q_z)$ can be rewritten in the concise form

$$S(Q_z) = S_M(Q_z) S_0 \int dr_\perp \frac{1}{a_0^2} \sum_{n,k=0}^{N} \exp[iQ_z d(k-n)] F_k(Q_z) C_{kn}(Q_z, r_\perp) F_n(Q_z) \ . \tag{4.3}$$

Here S_0 is a constant,

$$F_n(Q_z) = \exp(-\tfrac{1}{2} Q_z^2 \langle u_n^2 \rangle) \tag{4.4}$$

is the fluctuation term,

$$C_{kn}(Q_z, r_\perp) = \exp[Q_z^2 \langle u_k(\mathbf{r}_\perp) u_n(0) \rangle] \tag{4.5}$$

is the correlation term and

$$S_M(Q_z) = \left| \int dz \exp(iQ_z z) \rho_M(z) \right|^2 \tag{4.6}$$

is the molecular form factor. Although the fluctuation term may be viewed as an analog of the Debye-Waller factor in solids, its origin in smectic liquid crystals is different from that for the solids. Here the collective motion of molecules determines the value of $\langle u_n^2 \rangle$, whereas in solids it is the individual local vibrations of molecules.

To determine the contribution of each term to $S(Q_z)$, we can examine four interesting limits.. First by setting F_n, C_{kn}, and S_M equal to 1, the scattering for a one-dimensional solid consisting of $N+1$ δ-function scatterers is obtained; in this case there are no fluctuations, correlations, or molecular form factor so only the finite-size effects are present. Second by including F_n [calculated using Eqs. (3.7) and (4.4)], while keeping C_{kn} and S_M equal to 1, the influence of the layer fluctuations on the diffraction pattern of the one-dimensional solid is obtained. In this case, since $C_{kn} = 1$ each layer fluctuates independently from all the other layers. In the third and fourth cases, the correlation term C_{kn} and the molecular form factor S_M are included. For simplicity the calculations are shown for a very simple molecular electron density, uniformly distributed along the molecule. Then $\rho_M(z) = \Theta(|z| - L/2)$, where L is the length of the molecule, and S_M [see Eq. (4.6)] has a very simple form

$$S_M(Q_z) = \left| \frac{\sin(Q_z L/2)}{Q_z L/2} \right|^2 . \tag{4.7}$$

Although the molecular form factor for the real liquid-crystal molecule consisting of the benzene rings and hydrocarbon chains is much more complicated [27,42–45] than the simple form given by Eq. (4.7), it is sufficient to show the sensitivity of the x-ray diffraction pattern to the molecular form factor using the simple form. All the calculations were performed using typical values of the system parameters: $k_B T = 4 \times 10^{-14}$ erg, $K = 10^{-6}$ dyn, $B = 2.5 \times 10^7$ dyn/cm^2, $\gamma = 30$ dyn/cm, $d = 30$ Å, $L = 29$ Å, $a_0 = 4$ Å, $N_A = N + 1 = 3, 5, 11$ and $W = 4 \times 10^4$ Å.

Figure 6 shows the x-ray diffraction pattern for an ideal one-dimensional solid with 3,5,11 layers, respectively, and $F_n = C_{kn} = S_M = 1$. The scattering intensity in this case is given by the following simple formula:

$$S(Q_z) = S_0 \left[\frac{\sin(\frac{1}{2} N_A Q_z d)}{\sin(\frac{1}{2} Q_z d)} \right]^2 \frac{A}{a_0^2} \ , \tag{4.8}$$

where A is the area of the sample (for simplicity we set $A = \pi W^2$). This pattern is like the N-slit diffraction pattern known from optics. There are $N_A - 2$ subsidiary maxima between each pair of primary maxima. The primary maxima are located at $Q_z = 2\pi m/d$ for $m = 0, 1, 2 \ldots$ and do not depend on the number of layers. They are twice as wide as the subsidiary maxima. The minima of $S(Q_z)$ are located at $Q_z = 2\pi m/(N_A d)$, for any integer m indivisible by N_A (which is the number of layers). As we can see, the location of the minima is strongly size dependent, thus it can be used to determine the number of smectic layers in the film. In this case, the scattering at the minima of $S(Q_z)$ [Eq. (4.8)] is zero. In the limit of the infinitely large sample this structure evolves towards the pattern consisting of true δ Bragg peaks located at $Q_z = 2\pi m/d$.

Figure 7 shows the effects of including the fluctuations in the same system. The displacement fluctuations reduce the intensity of the scattering [now for $Q_z > 1.5$ Å^{-1} $S(Q_z) < 1$] and shift the locations of the scattering intensity minima, but the minima still go to zero. The fluctuations also change the widths of the primary maxima, but not their positions; for large Q_z they become equal to the subsidiary maxima widths. The latter effect is due to the fact that each layer has a different fluctuation amplitude (see Fig. 1). If the fluctuations were the same for each layer the fluctuation term given by Eq. (4.4) would simply multiply the ideal contribution and so could not change the locations of the scattering minima. In thin films the fluctuation amplitude has a profile and $\langle u_n^2 \rangle$ strongly depends on n (Fig. 1). The structure presented in Fig. 7 should in the limit of the infinitely large thickness (but finite transverse dimension) evolve to-

wards the pattern consisting of the quasi-Bragg-peaks of height decreasing like the Gaussian factor [see Eq. (4.4)] with the layer fluctuations given by Eq. (2.5). In the truly infinite sample there would be no scattering from the sample, because of the diverging fluctuations (see Sec. I). The smectic system, in this approximation, would then behave like the truly isotropic liquid.

Figure 8 shows the calculated scattering pattern when both the fluctuations and the correlations between layers are included (so now only $S_M=1$). First note that the correlation term C_{kn} is responsible for the diffuse scattering from the film; it produces the nonzero values of the intensities at the minima. However, it hardly changes the Bragg peaks located at the top of the diffuse scattering (compare Fig. 7 and Fig. 8). The maxima of the diffuse scattering for large N_A ($N_A>5$) are located at the same Q_z as the primary maxima. For the three-layer-thick film the diffuse scattering pattern is almost featureless. The

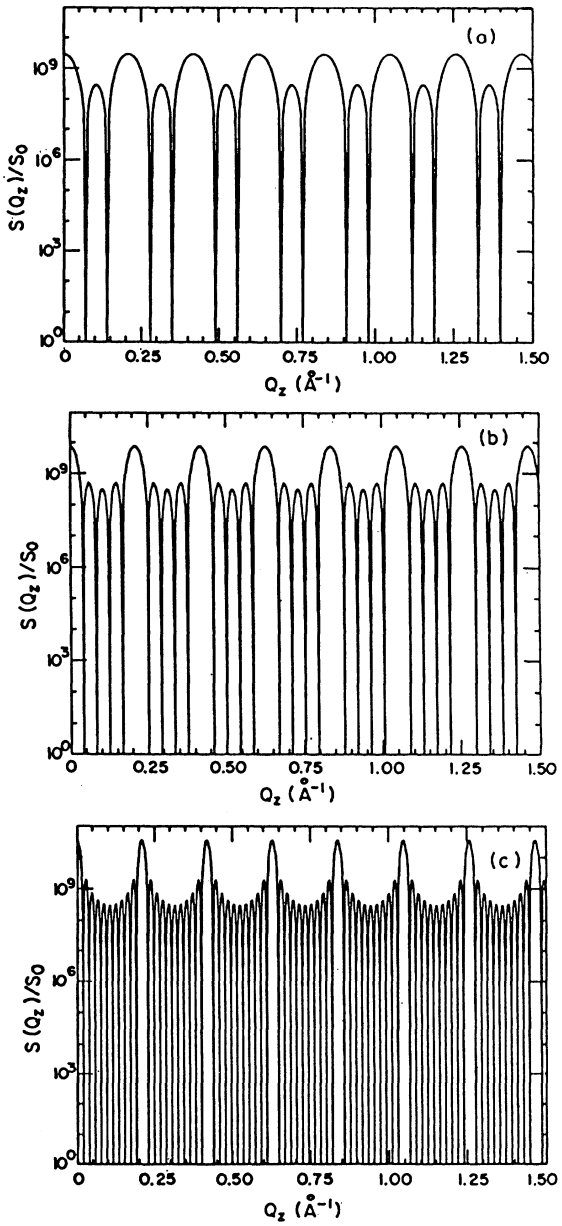

FIG. 6. X-ray-diffraction pattern for (a) a 3-layer, (b) a 5-layer, and (c) an 11-layer smectic film showing the effect of the finite size without the effects of the fluctuations, correlations, and the molecular form factor. The smectic period is $d=30$ Å.

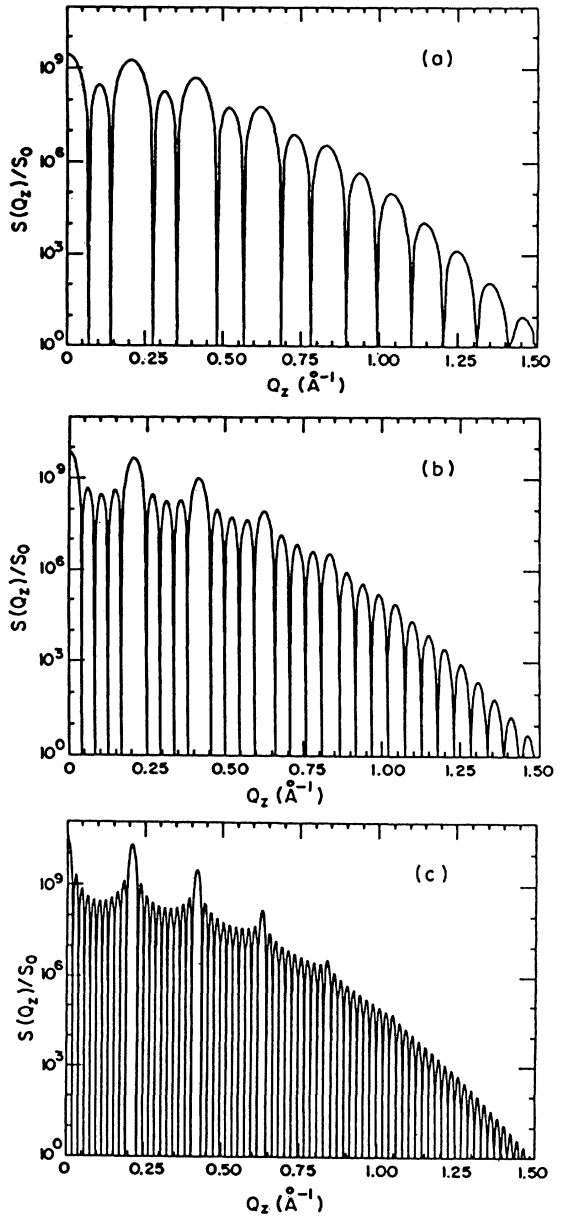

FIG. 7. X-ray-diffraction pattern for (a) a 3-layer, (b) a 5-layer, and (c) an 11-layer smectic film including the fluctuations, but not the correlations or the molecular form factor. Here $B=2.5\times10^7$ dyn/cm^2, $K=10^{-6}$ dyn, and $\gamma=30$ dyn/cm and d is the same as in Fig. 6.

envelopes of the minima for the scattering intensities presented in Fig. 8 are shown for 3-, 5-, 11-layer-thick films in Fig. 9. This represents the effect of the correlation alone. We note that this structure evolves from almost the featureless pattern for a 3-layer thick film to a well-developed pattern with well-visible maxima for an 11-layer thick film. Surprisingly there are at least four well-pronounced maxima in the correlation scattering pattern shown in Figs. 8(c) and 9 for an 11-layer-thick film, whereas we know from the large sample asymptotic

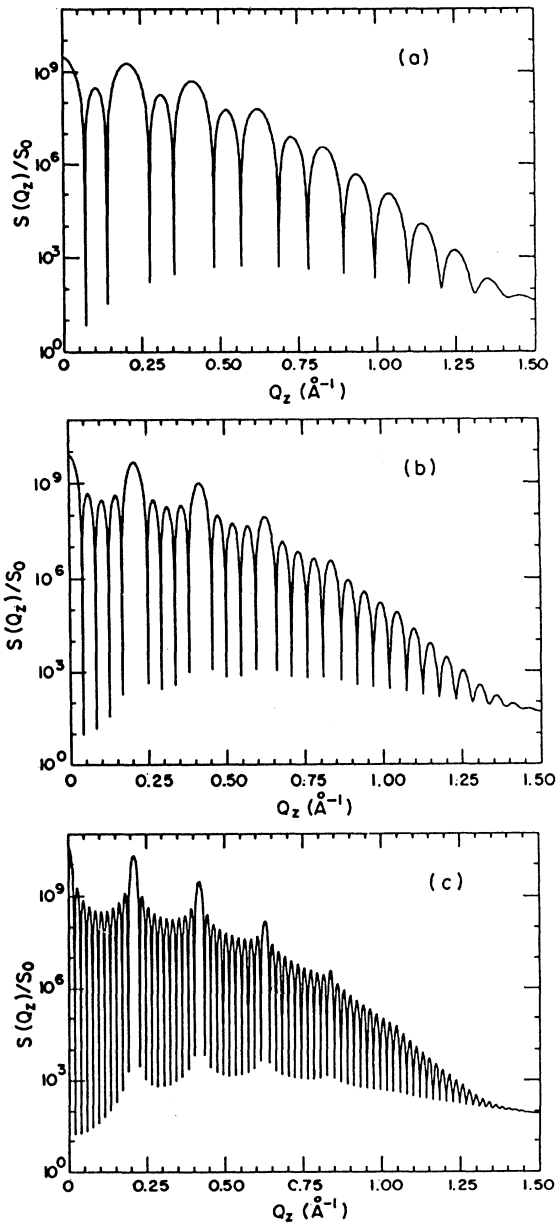

FIG. 8. X-ray-diffraction pattern for (a) a 3-layer, (b) a 5-layer, and (c) an 11-layer smectic film including both the fluctuations and the correlations, but not the molecular form factor. Smectic parameters as in Fig. 7.

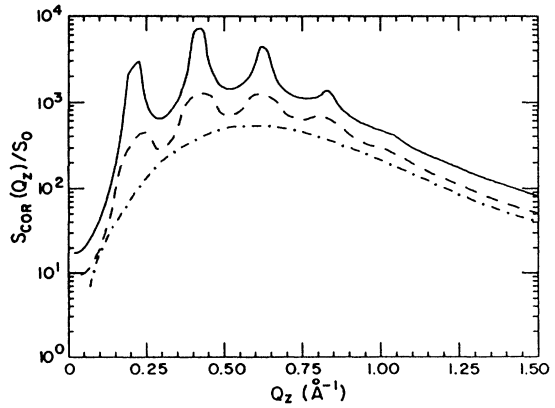

FIG. 9. The envelopes of the minima presented in Fig. 8. This shows the diffuse scattering intensity due to correlations for a 3-layer smectic film (dash-dotted line), a 5-layer smectic film (dashed line), and an 11-layer smectic film (solid line).

expansion for the scattering intensities [see Eq. (2.6) discussion below this equation] that the fourth peak should be absent. Thus we conclude that although the structure presented in Fig. 8(c) is very similar to the structure predicted for large samples by Gunther, Imry, and Lajzerowicz [36] it still has not reached the asymptotic limit. On the other hand, the asymptotic expansion for a finite sample is probably too simplified to predict the exact behavior of the high Q_z scattering intensity peaks. Also note that for $Q_z > 1.5$ Å^{-1} there is still an appreciable amount of diffuse scattering tail which only slowly goes to zero as Q_z increases. For $Q_z > 3$ Å^{-1} the scattering intensity is practically zero. In the limit of the infinite sample this scattering pattern evolves towards the structure given by Eq. (2.6) where instead of the Bragg peaks we have the power-law divergences at $Q_z = 2\pi m/d$ (Sec. II).

Figure 10 shows the full scattering pattern for S_M given by Eq. (4.7). Note that the molecular form factor greatly decreases the intensity of the scattering especially for $Q_z > 1.25$ Å^{-1} Also, because the length of the molecule, $L = 29$ Å, is only slightly smaller than the layer spacing, $d = 30$ Å, the molecular form factor has a minimum just past each primary maximum. In the case shown, it clearly splits the first primary maximum into two pieces. The envelopes of the subsidiary maxima and minima both follow the shape of the molecular form factor; this is very clear past the first primary maximum. This pattern certainly provides information about the length of the molecule and also in the case of the more complicated molecular structure about its location in smectic layers, and about its conformation.

V. DISCUSSION

A. Practical implications of the presented analysis and comparison with experiment

There are several practical implications of this analysis: Because the fluctuation term [Eq. (4.4)] and the

molecular form factor [Eq. (4.6)] strongly influence the x-ray diffraction pattern, both can be determined. In addition, because S_M depends on the locations of the atoms in the molecule, accurate intensity measurements for known molecules should allow determination of the conformation of these molecules in thin smectic films. As pointed out in the previous sections, since $\langle u_n^2 \rangle$ depends on K, B, and γ, these parameters can also be determined from the x-ray-diffraction pattern. In order to see the sensitivity of the x-ray-diffraction pattern to γ and B, we made a calculation of the x-ray-diffraction pattern for the small surface tension with other parameters unchanged [now $\gamma=5$ dyn/cm), shown in Fig. 11(a) and also for small B (now $B=0.25\times10^7$ dyn/cm^2] shown in Fig. 11(b). In order to understand all the differences between Figs. 11(a), 11(b), and Fig. 8(c), we have to recall the fluctuation profiles for all three cases. For the case of $\gamma=5$ dyn/cm [Fig. 1(b) for the profile and Fig. 11(a) for the corresponding scattering intensity] the average fluctuation amplitude is ~ 6 Å which is enough to reduce considerably the intensity of the quasi-Bragg-peaks after the third peak. Thus now the x-ray-scattering pattern is dominated by the correlation effects for $Q_z > 0.5$ Å^{-1}. Note that because the profile of the fluctuations shown in Fig. 1(b) is very weak the width of the primary maxima are practically unchanged in this case. On the contrary, for small B [Fig. 2(b) for the fluctuation profile and Fig. 11(b) for the correspond scattering intensity] the width of the second peak is practically indistinguishable from the width of the subsidiary minima. This is caused by the

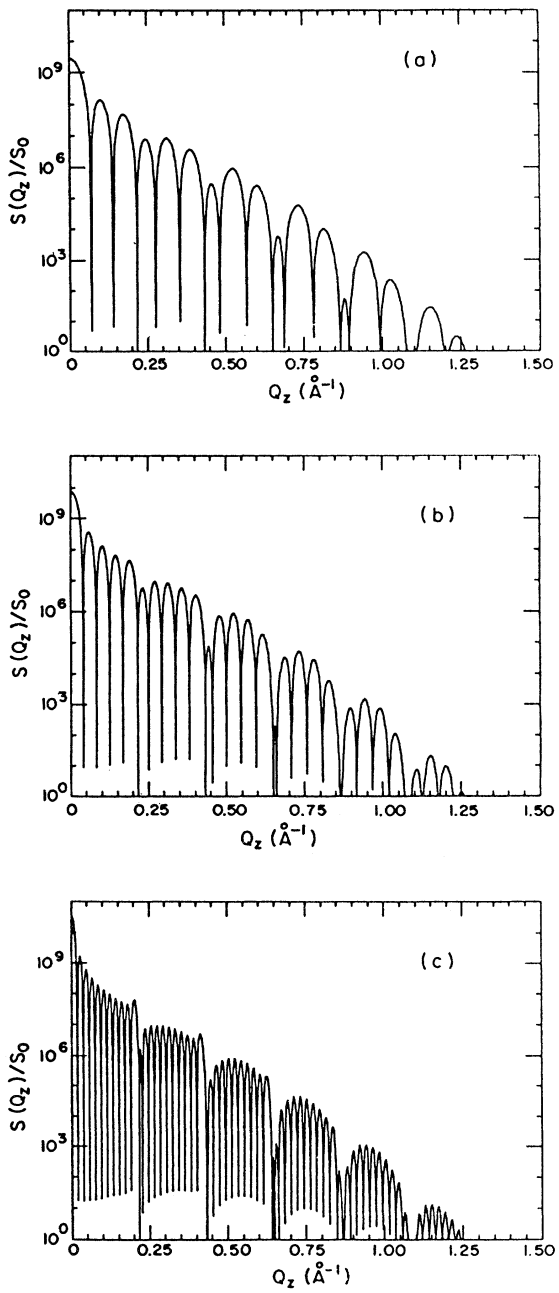

FIG. 10. X-ray-diffraction pattern for (a) a 3-layer, (b) a 5-layer, and (c) an 11-layer smectic film, showing the combined effect of finite size of the sample, fluctuations, correlations, and the molecular form factor. Smectic parameters as in Fig. 7.

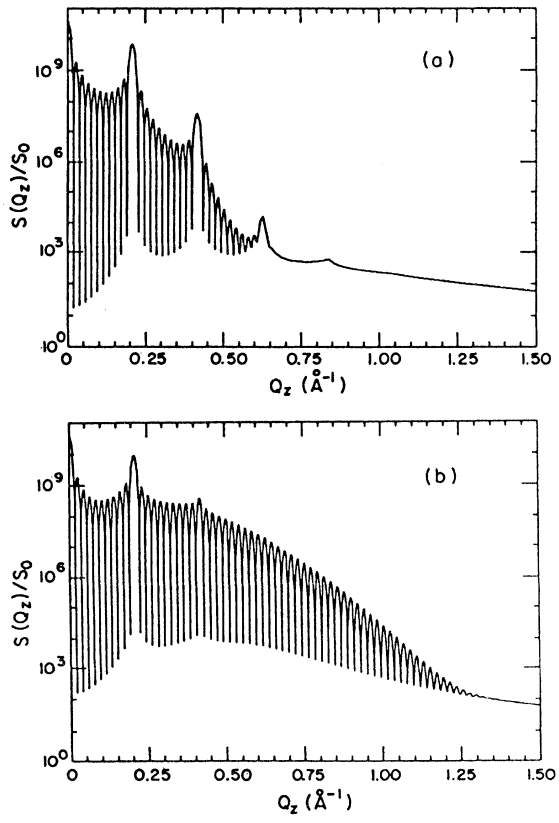

FIG. 11. X-ray-diffraction pattern for an 11-layer thick film with $K=10^{-6}$ dyn and (a) small surface tension, $\gamma=5$ dyn/cm. Here $B=2.5\times10^7$ dyn/cm^2; (b) a small B, $B=0.25\times10^7$ dyn/cm^2. Here $\gamma=30$ dyn/cm. The molecular factor is not included. This figure should be compared with Fig. 8(c).

very sharp fluctuation profile. Moreover, although the fluctuation amplitudes in the middle of the film (~ 8 Å) are larger than in the previous case of the small γ the fluctuation amplitudes at the surface are still very small (~ 3 Å) and that is why there is no sudden drop in the scattering intensity for large Q_z (see Fig. 11). Note that in both cases these large fluctuations do not very much affect the scattering due to correlations which is clear by comparing Fig. 11 with Fig. 8(c). However, in both cases, the change in the quasi-Bragg-peaks both in the primary and in the subsidiary maxima is large enough to be measured. The sensitivity of the x-ray-diffraction pattern to the layer fluctuation profile is fully investigated in the papers by Tweet *et al.* [27,45].

The correlation term given by Eq. (4.5) has very little effect on the scattering intensity in thin films since it does not change the Bragg peaks and, moreover, the ratio of the maximum diffuse scattering intensity to the first primary maximum intensity is less than 10^{-6}, so it is too small to be measured. In addition, because the resolution function obscures the details of the scattering pattern close to the minima [27,28,45], the effect of C_{kn} there will also be very difficult to observe. Consequently, the approximation $C_{kn}=1$ is adequate for the analysis of all thin-film experimental work. Indeed this assumption has been used with success in the theoretical analysis of the Tweet *et al* [27,45] experimental results. The experimental sample was the freely suspended film 7.O7 consisting of two hexatic, tilted smectic-I surface layers and the interior liquid, tilted smectic-C layers. In Appendix B the theory for the layer fluctuations which has been used to interpret the experimental data [45] is presented. Because the surface smectic-I layers are different than the interior smectic-C layers the theory for smectic-A presented in Sec. III had to be slightly modified. It has been possible to extract from the experimental data the following parameters: $\sqrt{K_C B_C}=3.14\pm 0.10$ dyn/cm, $(\gamma\sqrt{K_I B_{I\text{-}C}})^{1/2}=6.5\pm 0.5$ dyn/cm, and $8\geq\gamma\geq 3$ dyn/cm, where the subscript C stands for the smectic-C phase and I for the smectic-I phase. $B_{I\text{-}C}$ is the smectic elastic constant associated with the coupling between the surface smectic-I layer and the next smectic-C layer. The smectic-I elastic constants are about two times larger than those for smectic-C and consequently the smectic-I layers are much stiffer than smectic-C ones. We have neglected the coupling between the hexatic order parameter and the layer fluctuation amplitude in the free energy [46], assuming that the main effect of the hexatic order has been to increase the smectic elastic constants K_I and $B_{I\text{-}C}$ in comparison to the liquid smectic-C ones. In Ref. [27] the anisotropy of the real-space cutoff W introduced a considerable overestimate in the determination of the surface tension and the elastic constants. It has been corrected in Ref. [45]. Here we give the corrected values of the smectic parameters.

Finally we would like to point out that the presented model can be also applied to the experiment performed by Gierlotka, Lambooy, and de Jeu [28] on thin freely suspended smectic-A_d film. In Appendix C we give the explicit form for the scattering intensity in this case.

B. Approximations made in the model

Although the $|\nabla u|^2$ term should, in principle, appear for each layer, because the rotational symmetry has been broken by the film holder, we have assumed that for the interior layers the contribution of this term to the free energy is very small. In the first approximation this term should be proportional to the square of the density difference between layers [47]. For the surface layer, where the density difference between liquid-crystal liquid and its vapor is huge, this term which we identify with the surface tension is large, whereas for the interior layers, where the density difference is a few percent at most, this term can be neglected. We have also not included the anharmonic terms in the free energy, because they should not affect the fluctuations very much (see discussion in Sec. II), and also neglected the influence of the disjoining pressure to the free energy [48-51]. This effect is probably small; according to the recent measurements for lyotropic lamellar mesophases between two mica surfaces [52] the contribution of the disjoining pressure to the surface tension is ~ 1 dyn/cm. This is within the experimental error. In the model we have also neglected the coupling between the director fluctuations and the layer fluctuations and the influence of the tilt profile on the layer fluctuations. The coupling between the director fluctuations and layer fluctuations may be easily included and is presented in Sec. V E.

C. Individual versus collective fluctuations; surface melting versus surface freezing

In addition to the hydrodynamic (collective), long-wavelength fluctuations which have been calculated in this paper, there are also short-wavelength contributions to the total fluctuation profile that should be properly included before comparing the theoretical predictions with experiment. These short-wavelength contributions are due to the individual motions of the molecules. Suppose that these molecular motions make the density distribution for the layer positions to be Gaussian (this is true for the harmonic Debye-Waller theory [53]) and that the long-wavelength fluctuations further broaden this Gaussian distribution. The density operator for the layer position (for simplicity we neglect the molecular form factor) can be written now in the following form:

$$\hat{\rho}=\rho_s \sum_{n=0}^{N} \frac{1}{(2\pi\sigma_L^2)^{1/2}} \exp\left[-\frac{[z-nd-u_n(\mathbf{r}_\perp)]^2}{2\sigma_L^2}\right] . \tag{5.1}$$

Here σ_L is the fluctuation amplitude due to the individual molecular motion and ρ_s is the number of molecules per unit surface area. The individual molecular fluctuation amplitude should be larger at the surface than in the bulk in contrast to the hydrodynamic fluctuations which are quenched by the surface tension. The profile of σ_L can be probably described by the mean-field density-functional theory for smectic phases [54–60]. Averaging $\hat{\rho}$ with the free energy given by the harmonic elastic mod-

el [Eq. (3.2)] we get the average layer density distribution

$$\rho(z)=\rho_s \sum_{n=0}^{N} \frac{1}{(2\pi\sigma^2)^{1/2}} \exp\left[-\frac{(z-nd)^2}{2\sigma^2}\right] . \quad (5.2)$$

Here

$$\sigma=(\sigma_L^2+\sigma_n^2)^{1/2} , \quad (5.3)$$

and the elastic fluctuations σ_n^2 are given by Eqs. (3.7)–(3.13). For $\sigma_n=4$ Å and $\sigma_L=1$ Å [61] (measured by Leadbetter, Mazid, and Richardson [61] using neutron scattering) we get $\sigma=4.12$ Å, so the individual molecular motion contributes only 0.12 Å to the layer fluctuation amplitudes and the hydrodynamic, long-wavelength contribution dominates. Although the Leadbetter, Mazid, and Richardson [61] measurements were performed for the crystalline smectic liquid crystals this value for the individual fluctuations should be similar in dense liquid smectic liquid crystals, because locally the dense liquid is very similar in structure to the solid phase. Below we discuss the implications of this analysis for the surface freezing [17] and surface melting transitions [62–67].

In 1910 Lindemann [68] formulated a useful criterion for melting, which asserts that melting occurs if the fluctuation amplitude σ of an atom exceeds 10% of the nearest-neighbor distance. In solids where the individual fluctuations dominate, atoms at the surface fluctuate more than the atoms in the bulk. This means that the criterion can be fulfilled for the surface atoms before it is fulfilled for the atoms inside the sample. Thus the melting transition can be initiated at the surface. In smectic liquid crystals it has been observed that surface freezing occurs [17] instead of surface melting. We interpret this result by the dominance of the hydrodynamic fluctuations over the local fluctuations. The hydrodynamic fluctuations are quenched at the surface; thus surface freezing rather than surface melting should occur in this case.

D. X-ray correlation length and the cutoff

As has been mentioned in Sec. III the cutoff W that appears in the model is not simply the size of the system, but rather is related to the properties of the x-ray beam. Here we would like to elaborate on this topic and give a rough estimate of the cutoff for the typical experimental setup [27,28]. In such experiments the x-ray radiation produced by the rotating anode is scattered from the monochromator (graphite [27] or germanium [28]), which produces the beam of well-defined $\mathbf{k}$ wave vector. According to the Bragg condition for scattering from crystals [53] only this $\mathbf{k}$ is selected which forms a definite angle with the crystal planes. However, the monochromator crystals are not perfect; thus the outgoing x-ray beam has some small angular spread in $\mathbf{k}$. This x-ray beam with the angular spread, α, may be viewed as if the radiation was produced by the incoherent extended source of spatial dimension R_1 at distance R from the sample, such that $\alpha=R_1/R$. Now consider the correlation between the electromagnetic field vibrations at two points at the surface of our sample, separated by the distance $r_\perp$. We denote this function $\mu=\langle A(r_\perp,t)A(0,t)\rangle$ and further neglect the retardation effects, which is justified providing the photon coherence length $c\tau_c$ is much greater than $r_\perp$. Here τ_c is the photon coherence time [69], c is the speed of light, $\langle\ \rangle$ denotes the time average, and $A(r_\perp,t)$ is the amplitude of the electromagnetic wave at point $r_\perp$ at time t. The distance $r_\perp$ over which μ is large and positive will be called the photon correlation length in order to distinguish it from the previously mentioned photon coherence length. One finds that μ is given by the Van Cittert-Zernike formula and for the circular source is proportional to [70] $2J_1(v)/v$, where J_1 is the Bessel function of the first kind, $v=2\pi r_\perp/\lambda$, and λ is the wavelength of the x-ray radiation. The maximum value of μ is 1 for $v=0$ and it reaches value 0.88 at $v=1$, i.e., when

$$r_\perp^*=0.16\lambda/\alpha . \quad (5.4)$$

This somehow arbitrary (we considered 12% deviation from the ideal value of μ) fixed length is a photon correlation length along the surface of the sample. This length is modified by the angle θ between the incoming beam and the surface. Taking this into account we finally find

$$r_\perp^*=0.16\lambda/(\alpha\sin\theta) . \quad (5.5)$$

For $\lambda\simeq1$ Å, $\alpha\simeq0.02°$, and $\theta\simeq1°$ we find $r_\perp^*\simeq10^4$ Å. Over distances larger than $r_\perp^*$ the photon is scattered incoherently and consequently the layer fluctuations characterized by the wavelength smaller than $q_\perp^*=2\pi/r_\perp^*$ cannot be detected. Thus it is natural to set the cutoff $W=r_\perp^*$ where $r_\perp^*$ is given by Eq. (5.5). In the real experiment [45] the cutoff strongly depends on the geometry and size of the slits which narrow the x-ray beam. In fact, in the experiment discussed [45] the correlation length has been shown to be anisotropic, i.e., the correlation length along the x axis, $W_x=400$ Å, while the one along the y axis, $W_y=40\,000$ Å. In the theoretical analysis of the experimental results [45] the correlation area has been approximated by the rectangle of size $2W_x$ and $2W_y$. In the simplest case considered in this paper the correlation area is a circle of radius W.

E. Coupling between layer and director fluctuations

The free energy associated with the director distortions is given by the Frank free energy [34]

$$F_{\rm dir}=\tfrac{1}{2}\{K_1[\nabla\mathbf{n}(\mathbf{r})]^2+K_2[\mathbf{n}(\mathbf{r})\nabla\times\mathbf{n}(\mathbf{r})]^2 +K_3[\mathbf{n}(\mathbf{r})\times\nabla\times\mathbf{n}(\mathbf{r})]^2\} , \quad (5.6)$$

where K_1 is the elastic constant associated with splay deformations, K_2 is the elastic constant associated with twist deformations, and K_3 is the elastic constant associated with bend deformations. As pointed out by de Gennes [34] if we assume that the director is perpendicular to layers and that the layer spacing does not change, the director fluctuations can be incorporated in the undulational mode. To be specific, the director, in this case, is simply given by the vector normal to the smectic layers and in the limit of small displacement gradients is equal to

$$\mathbf{n}(\mathbf{r})=\begin{bmatrix} -\dfrac{\partial u(\mathbf{r})}{\partial x} \\ -\dfrac{\partial u(\mathbf{r})}{\partial y} \\ 1 \end{bmatrix} . \tag{5.7}$$

Furthermore, if the layer is unaltered in the process of fluctuations the bend and twist contributions to the director distortions are forbidden and only splay contributes. Taking into account Eq. (5.7) it is easy to see that the splay term in Eq. (5.6) has the same structure as the undulational term in Eq. (2.2) [34]. All these assumptions are very reasonable providing there is no strong displacement fluctuation profile. However as has been pointed out in Sec. III B for very small smectic elastic constants and very large surface tension the displacement gradients are very large and the presented theory is no longer valid. The direct distortions have to be included in this case. The coupling between the undulational mode and the director fluctuations is given by

$$F_{\text{coup}}=K_{\text{coup}}[\mathbf{n}(\mathbf{r})-\mathbf{e}_z(\mathbf{r})]^2 , \tag{5.8}$$

where $\mathbf{e}_z$ is the vector normal to the layers. In the simplest approximation $\mathbf{e}_z$ is given by Eq. (5.7).

F. Fluctuation induced tilt profiles and smectic-A–smectic-C phase transition in thin films

In this section we would like to speculate on the possible influence of the fluctuation profile on the tilt profile observed in thin tilted smectic films [27,45] and on the smectic-A–smectic-C phase transitions in very thin films [71]. First we will analyze the structure of the bulk smectic liquid crystals and further discuss its implications for the structure of thin smectic films.

In the smectic-A phase the director is perpendicular to the layers but the molecules are not perfectly aligned. The nematic order parameter

$$Q_N=\frac{1}{2M}\left\langle \sum_{i=1}^{M}[3\cos^2(\phi_i)-1]\right\rangle \tag{5.9}$$

is less than 1 (its maximal value for a perfectly aligned sample), nonetheless it is very large (usually $Q_N>0.9$). Here $\langle\ \rangle$ denotes the statistical average, ϕ_i is the angle between the director and the long axis of the ith molecule, and M is the number of molecules. In the case of smectic-A liquid crystals one can interpret

$$\phi^*=\arccos\left[\left[\frac{1}{M}\sum_{i=1}^{M}\langle\cos^2(\phi_i)\rangle\right]^{1/2}\right] \tag{5.10}$$

as an average angle between the long axis of the molecule and the normal to the layer. The molecules in smectic-A liquid crystals freely rotate around the normal to the layers. In smectic-C liquid crystals rotations are frozen, axial symmetry is broken, and ϕ^* is the tilt angle (the angle between the director and the normal to the layers). Of course the molecules in the smectic-C phase still rotate freely around the director, but the director is no longer perpendicular to the layers. Why is Q_N so large (or equivalently ϕ^* so small) in the smectic-A phase? The answer to this question has been given in the framework of the density-functional theory [57] for the nematic–smectic-A (N–Sm-A) phase transition and is also presented below. The rotational motion strongly hinders the translational motion inside layers and only if Q_N is large (ϕ^* is small) this effect is small and the entropy gained in the process of layer formation (at the N–Sm-A phase transition) can outweigh the entropy loss associated with it. Namely, the molecules inside layers have more translational freedom than they had in the nematic phase and this accounts for the entropy gain; on the other hand, the molecules cannot move freely between layers which accounts for the entropy loss [57]. The condition of large Q_N (small ϕ^*) in bulk smectics liquid crystals has important consequences in thin smectic films with the strong fluctuation profile as shown below.

The existence of the fluctuation profile in thin smectic films means that neighboring layers fluctuate with different amplitudes. The compressional mode due to these differences in amplitudes induces the change in the layer spacing, d. The change in d can be achieved in smectic liquid crystals in two ways. One is the interpenetration of molecules from neighboring layers, the other is the change in ϕ^* because

$$d\approx L|\cos\phi^*| , \tag{5.11}$$

where L is the length of a molecule. The former mechanism is less probable because of the high entropy cost associated with the interpenetration [57]. Thus we are left with the latter mechanism. In particular, from this mechanism one can predict that the layer fluctuation profile induces the ϕ^* profile. Moreover, for very large layer fluctuation gradients the change in ϕ^* can be very large. If ϕ^* for a given layer is too large the rotations around the director very strongly hinder the translational motion inside this layer, as mentioned previously in the discussion of Q_N. The only way to change this unfavorable configuration is to freeze rotations for all the molecules inside the layer. But this leads to the smectic-A–smectic-C phase transition indeed observed in very recent optical experiments in very thin smectic-A films [71].

The tilt profile changes the layer spacing as indicated in the condition (5.11) and thus moves the scattering peaks. This property has been used to determine the tilt profile from x-ray diffraction pattern in the smectic-I and $-C$ films [27,45]. The tilt and displacement fluctuation profiles observed in these experiments agree qualitatively with the hypothesis presented above. According to it both the tilt profile and the fluctuation profile arise because of the presence of the surface tension, which by quenching the surface fluctuations induces the fluctuation profile and eventually the tilt profile. It may also be true that large tilt at the surface produced by the surface tension initiated the liquid-hexatic phase transition (smectic-C–smectic-I) in the surface layer. The conclusive experimental proof of this mechanism for the fluctuation-induced tilt profile could be obtained from the x-ray-diffraction pattern for thin smectic-A films.

G. Effect of small surface tension and small real-space cutoff on the fluctuation profiles

So far we have confined our analysis to the typical values of the elastic constants, K, B, the surface tension γ, and the real-space cutoff W. Now we would like to discuss the two interesting cases of small W and small γ.

The fluctuations in the center of the film grow logarithmically with its thickness, D_z, and for large W ($W \gg D_z$) and large D_z have the form (2.3). By comparison of Eq. (2.3) and Eq. (2.5) we find that for $D_z \approx W^2/\lambda$ the fluctuations in the center of the film should saturate (stop growing). However, in the case of small W ($W/a_0 \approx 100$) the above analysis does not apply. In particular, the saturation of the fluctuations in the center is observed at $D_z \approx W$. Moreover, the saturated profile is very flat in the middle (in contrast to the parabolic profile discussed in detail in the paper) and its shape can be reproduced by the hyperbolic cosine [72]. This observation may be very useful in the analysis of experimental data, namely, the hyperbolic cosine form (obtained from the saturated profiles for thin films) can be used to fit the data even for the very thick films.

The case of very small surface tension ($\gamma \ll \sqrt{KB}$) may be relevant to the finite system of stacked membranes [73]. We observed that in such a system the fluctuations at the surface are *larger* than the fluctuations in the interior. Moreover, the fluctuations *decrease* with the thickness of the film. This behavior is completely opposite to the one studied in the previous sections. The reason for this behavior is the fact that small surface tension cannot compensate for the increase of fluctuations due to the lack of one nearest-neighbor layer for the surface layer. So the surface layer will fluctuate more than the interior. The decrease of the fluctuations with the thickness is also understandable by the same token. Finally we note that the behavior of the fluctuations in thin films can be even more complicated for the stratified systems with small surface tension and two different sets of elastic constants at the surface (K_s, B_s) and in the interior (K_b, B_b) like in the smectic-*I* on -*C*. In particular, for $\gamma \ll \sqrt{K_b B_b}$ and $\sqrt{K_b B_b} \ll \sqrt{K_s B_s}$ such that $(\gamma \sqrt{K_s B_s})^{1/2} \geq \sqrt{K_b B_b}$ the fluctuations first grow with the thickness of the film for very thin films and then, for thicker films, decrease with the thickness of the film.

I hope that the presented analysis will be a good starting point for future experimental and theoretical studies of thin smectic systems.

ACKNOWLEDGMENTS

I would like to thank Professor Michael Schick, Professor Larry Sorensen, and Professor Herbert Wagner for interesting suggestions. I am very grateful to Professor Larry Sorensen and Dr. Douglas Tweet for many fruitful discussions and for introducing me to the world of x-ray experiments. I also acknowledge interesting discussions with Brian Swanson and Hans Stragier. This work was supported by the National Science Foundation under Grants No. DMR-8916052 and No. DMR-8612286.

APPENDIX A: INVERSION OF THE MATRIX $\underline{M}$

According to the definition, the elements of the inverse matrix $(\underline{M}^{-1})^{(N+1)}$ are given by

$$(\underline{M}^{-1})^{N+1}_{kn} = (-1)^{n+k} \frac{\det \underline{\tilde{M}}^{(N)}_{kn}}{\det \underline{M}^{(N+1)}} \ . \tag{A1}$$

Here the matrix $\underline{\tilde{M}}^{(N)}_{kn}$ is obtained from $\underline{M}^{(N+1)}$ by deleting the kth column and the nth row and det denotes the determinant. The superscript indicates the dimension of the matrix. Let the square matrix $\underline{M}^{(N+1)}$ have only the following nonzero elements:

$$M_{00} = M_{NN} = a \ , \tag{A2}$$

$$M_{nn} = b \ , \tag{A3}$$

$$M_{n+1n} = M_{nn+1} = c \ , \tag{A4}$$

Expanding the determinant of $\underline{M}^{(N+1)}$ in the first and last row elements we easily get

$$\det \underline{M}^{(N+1)} = a^2 \det \underline{T}^{(N-1)} - 2ac^2 \det \underline{T}^{(N-2)} + c^4 \det \underline{T}^{(N-3)} \ . \tag{A5}$$

Here the matrix $\underline{T}^{(J)}$ has, for any J, the following elements:

$$(\underline{T}^{(J)})_{kn} = c\delta_{k,n+1} + c\delta_{k+1,n} + b\delta_{k,n} \ , \tag{A6}$$

for any n and k, and δ stands for Kronecker's δ function. Now let

$$\underline{T}^{(J)} = b^J \underline{L}^{(J)} \ . \tag{A7}$$

It is easy to verify, by expanding the matrix $\underline{L}^{(J)}$ in the first row elements, that the following recursive relation is satisfied:

$$\det \underline{L}^{(J)} = \det \underline{L}^{(J-1)} - \alpha^2 \det \underline{L}^{(J-2)} \ , \tag{A8}$$

where $\alpha = c/b$. From this equation we also get the following relation:

$$\begin{bmatrix} \det \underline{L}^{(J)} \\ \det \underline{L}^{(J-1)} \end{bmatrix} = \begin{bmatrix} 1 & -\alpha^2 \\ 1 & 0 \end{bmatrix} \begin{bmatrix} \det \underline{L}^{(J-1)} \\ \det \underline{L}^{(J-2)} \end{bmatrix} \ . \tag{A9}$$

This equation can be solved iteratively. For $J = 0$ and 1 we have $\det \underline{L}^{(J)} = 1$, thus

$$\begin{bmatrix} \det \underline{L}^{(J)} \\ \det \underline{L}^{(J-1)} \end{bmatrix} = \begin{bmatrix} 1 & -\alpha^2 \\ 1 & 0 \end{bmatrix}^{J-1} \begin{bmatrix} 1 \\ 1 \end{bmatrix} \ . \tag{A10}$$

Diagonalizing the matrix in Eq. (A10) one easily finds that

$$\begin{bmatrix} 1 & -\alpha^2 \\ 1 & 0 \end{bmatrix}^{J-1} = \underline{S}^{-1} \begin{bmatrix} \eta_+ & 0 \\ 0 & \eta_- \end{bmatrix}^{J-1} \underline{S} \ , \tag{A11}$$

where

$$\underline{S} = \begin{bmatrix} 1 & -\dfrac{\alpha^2}{\eta_+} \\ 1 & -\dfrac{\alpha^2}{\eta_-} \end{bmatrix} \ , \tag{A12}$$

and

$$\eta_{\pm}=\frac{1\pm[1-4(c/b)^2]^{1/2}}{2} . \tag{A13}$$

Combining Eqs. (A7)–(A13) we get

$$\det\underline{T}^{(J)}=b^J\frac{\eta_+^{J+1}-\eta_-^{J+1}}{\eta_+-\eta_-} . \tag{A14}$$

It is also easy to show that

$$\det\underline{\tilde{M}}^{(N)}_{nk}=\det\underline{A}^{(k)}c^{|n-k|}\det\underline{A}^{(N-n)} , \tag{A15}$$

for $n\geq k$, otherwise n and k should be exchanged. Here

$$\det\underline{A}^{(J)}=a\,\det\underline{T}^{(J-1)}-c^2\det\underline{T}^{(J-2)} .$$

Combining Eqs. (A14)–(A16) we get Eqs. (3.9)–(3.15). For $J=0$ we set $\det\underline{A}^{(J)}=1$.

APPENDIX B: THE FORMULA FOR THE FLUCTUATION PROFILE IN THE SMECTIC-*I* ON -*C* SYSTEM

Here we present the results for the smectic-*I* on -C system studied experimentally by Tweet *et al.* [27,45]. The experimental sample consisted of two surface smectic-*I* and the interior smectic-*C* layers. The total number of layers is $N+1$. The formula for the fluctuation profile is given in this case by the same equation as for smectic-*A* [Eq. (3.7)], but with different $N+1\times N+1$ matrix $\underline{M}$:

$$M=\begin{pmatrix}
a_1 & c_1 & 0 & 0 & 0 & \cdots & 0 & 0 & 0 & 0 & 0\\
c_1 & b_1 & c & 0 & 0 & \cdots & 0 & 0 & 0 & 0 & 0\\
0 & c & b & c & 0 & \cdots & 0 & 0 & 0 & 0 & 0\\
0 & 0 & c & b & c & \cdots & 0 & 0 & 0 & 0 & 0\\
0 & 0 & 0 & c & b & \cdots & 0 & 0 & 0 & 0 & 0\\
\vdots & \vdots & \vdots & \vdots & \vdots & \ddots & \vdots & \vdots & \vdots & \vdots & \vdots\\
0 & 0 & 0 & 0 & 0 & \cdots & b & c & 0 & 0 & 0\\
0 & 0 & 0 & 0 & 0 & \cdots & c & b & c & 0 & 0\\
0 & 0 & 0 & 0 & 0 & \cdots & 0 & c & b & c & 0\\
0 & 0 & 0 & 0 & 0 & \cdots & 0 & 0 & c & b_1 & c_1\\
0 & 0 & 0 & 0 & 0 & \cdots & 0 & 0 & 0 & c_1 & a_1
\end{pmatrix} , \tag{B1}$$

where

$$a_1=\gamma q_\perp^2+K_1dq_\perp^4+\frac{B_{I\text{-}C}}{d} , \tag{B2}$$

$$b_1=K_Cdq_\perp^4+\frac{B_{I\text{-}C}+B_C}{d} , \tag{B3}$$

$$c_1=-\frac{B_{I\text{-}C}}{d} , \tag{B4}$$

$$c=-\frac{B_C}{d} , \tag{B5}$$

$$b=K_Cdq_\perp^4+\frac{2B_C}{d} . \tag{B6}$$

Here K_I is the smectic elastic constant for smectic-*I* film and $B_{I\text{-}C}$ is the smectic elastic constant associated with compressional modes between the layer of smectic-*I* film and the layer of smectic-*C* film. We note that for the three-layer film the form of b_1 is slightly different, i.e.,

$$b_1=K_Cdq_\perp^4+\frac{2B_{I\text{-}C}}{d} . \tag{B7}$$

The elements of the inverse matrix $(\underline{M}^{-1})^{(N+1)}$ are given by (Appendix A)

$$(\underline{M}^{-1})^{(N+1)}_{nn}=\frac{\det\underline{A}^{(n)}\det\underline{A}^{(N-n)}}{\det\underline{M}^{(N+1)}} . \tag{B8}$$

Here the superscript stands for the dimension of the matrix. For $N>3$ and $N-1\geq n>1$ we have

$$\begin{aligned}\det\underline{M}^{(N+1)}=&(a_1b_1-c_1^2)^2\det\underline{T}^{(N-3)}\\&-2a_1c^2(a_1b_1-c_1^2)\det\underline{T}^{(N-4)}\\&+a_1^2c^4\det\underline{T}^{(N-5)} ,\end{aligned} \tag{B9}$$

and

$$\det\underline{A}^{(n)}=(a_1b_1-c_1^2)\det\underline{T}^{(n-2)}-a_1c^2\det\underline{T}^{(n-3)} , \tag{B10}$$

and the determinant of $\underline{T}$ is given in Appendix A. For $n=1$ $\det\underline{A}^{(n)}=a_1$. The cases $N=2,3$ (three- and four-layer-thick film) require separate formulas. Because the dimensionality of these matrices is low these formulas can be obtained immediately. Also the cases $n=0,N$ require separate formulas. They are given below.

$$\begin{aligned}\det\underline{A}^{(N)}=&b_1(a_1b_1-c_1^2)\det\underline{T}^{(N-3)}\\&-c^2(2a_1b_1-c_1^2)\det\underline{T}^{(N-4)}\\&+a_1c^4\det\underline{T}^{(N-5)} ,\end{aligned} \tag{B11}$$

and $\det\underline{A}^{(0)}=1$. Combining these formulas and Eq. (3.7) one can obtain the fluctuation profiles by simple numerical integration.

APPENDIX C: X-RAY-SCATTERING INTENSITY FOR SMECTIC-A_d FILMS

The smectic-A_d phase is drawn schematically in Fig. 12. Its structure can be characterized by the superposition of two one-dimensional density waves (defining smectic layers) of different phases and polarizations, i.e., of the same basic smectic period d and shifted with respect to each other by the vector $d_1\mathbf{e}$, where $\mathbf{e}$ is the unit vector parallel to the z axis [74]. In our convention when the arrow points up the polarization is positive, otherwise it is negative (Fig. 12). Of course two neighboring layers of opposite polarization form a bilayer. The scattering intensity $S(Q_z)$ is given by Eq. (4.1) with the density operator

$$\begin{aligned}\hat{\rho}(\mathbf{r})=&\rho_s\sum_{n=0}^{N}\int dz'\delta(z-z'-nd-u_n(\mathbf{r}_\perp))\rho_M^{(1)}(z')\\&+\rho_s\sum_{n'=0}^{N}\int dz'\delta(z-z'-n'd-d_1u_{n'}(\mathbf{r}_\perp))\rho_M^{(2)}(z') .\end{aligned} \tag{C1}$$

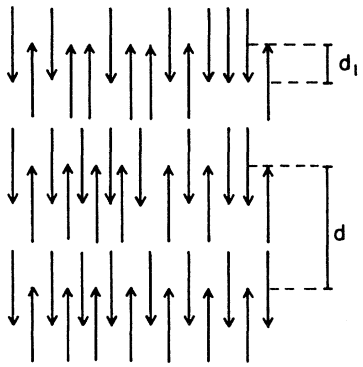

FIG. 12. Schematic drawing of the smectic-A_d phase; d is the smectic period and d_1 is the shift of the density waves. The arrows denote the polar molecules in smectic layers.

In the first term in Eq. (C1) the summation is over the indices of the monolayers with positive polarization and the summation in the second term is over the indices of the monolayers with negative polarization. The molecular density operator $\rho_M^{(i)}$ is different for the layers with positive polarization ($i=1$) from the one for the layers with negative polarization ($i=2$), but also satisfies the following relation:

$$\rho_M^{(1)}(z)=\rho_M^{(2)}(-z) \ . \tag{C2}$$

Combining the definition of $S(Q_z)$ given by Eqs. (4.1) and (C1) we get the scattering intensity for the smectic-A_d film,

$$S(Q_z)=S_M(Q_z)S_0\int d\mathbf{r}_\perp \frac{1}{a^2}\sum_{n,k=0}^{N}\exp[iQ_z d(k-n)] \times F_k(Q_z)C_{kn}(Q_z,r_\perp) \times F_n(Q_z) \ , \tag{C3}$$

where now the summations run over the indices of bilayers and the molecular form factor is equal to

$$S_M(Q_z)=|\rho_M^{(1)}(Q_z)|^2+|\rho_M^{(2)}(Q_z)|^2 +\rho_M^{(1)}(Q_z)\rho_M^{*(2)}(Q_z)\exp(-iQ_z d_1) +\rho_M^{*(1)}(Q_z)\rho_M^{(2)}(Q_z)\exp(iQ_z d_1) \ . \tag{C4}$$

Here * denotes the complex conjugated and $\rho_M^{(i)}(Q_z)$ for $i=1,2$ is the Fourier transform of $\rho_M^{(i)}(z)$. The fluctuation term F_n and the correlation term C_{kn} are given by Eqs. (4.4) and (4.5) respectively, and the free energy is given by Eq. (3.2) with $N+1$ being the number of bilayers and K and B being the smectic elastic constants for a bilayer. Of course in the analysis of the experimental results the correlation term can be neglected. The presented model is the simplest one, however it is also very easy to incorporate other more complicated effects like the tilt profile and the change of d_1 with z. Both effects can be induced by the layer fluctuations and the fluctuations profile.

*Institute of Physical Chemistry of the Polish Academy of Sciences, Department III, Kasprzaka 44/52, 01224 Warsaw, Poland.

[1] C. Y. Young, R. Pindak, N. A. Clark, and R. B. Meyer, Phys. Rev. Lett. **40**, 773 (1978).
[2] C. Rosenblatt, R. Pindak, N. A. Clark, and R. B. Meyer, Phys. Rev. Lett. **42**, 1220 (1979).
[3] S. Heinekamp, R. A. Pelcovits, E. Fontes, E. Y. Chen, R. Pindak, and R. B. Meyer, Phys. Rev. Lett. **52**, 1017 (1984).
[4] S. B. Dierker and R. Pindak, Phys. Rev. Lett. **59**, 1002 (1987).
[5] S. Sprunt and J. D. Litster, Phys. Rev. Lett. **59**, 2682 (1987).
[6] M. Cheng, J. T. Ho, S. W. Hui, and R. Pindak, Phys. Rev. Lett. **59**, 1112 (1987); **60**, 862 (1988).
[7] R. Geer, C. C. Huang, R. Pindak, and J. W. Goodby, Phys. Rev. Lett. **63**, 540 (1989).
[8] D. E. Moncton and R. Pindak, Phys. Rev. Lett. **43**, 701 (1979).
[9] E. B. Sirota, P. S. Pershan, L. B. Sorensen, and J. Collett, Phys. Rev. A **36**, 2890 (1987).
[10] E. B. Sirota, P. S. Pershan, L. B. Sorensen, and J. Collett, Phys. Rev. Lett. **55**, 2039 (1985).
[11] J. Collett, P. S. Pershan, E. B. Sirota, and L. B. Sorensen, Phys. Rev. Lett. **52**, 356 (1984).
[12] J. D. Brock, A. Aharony, R. J. Birgeneau, K. W. Evans-Lutterodt, J. D. Litster, P. M. Horn, G. B. Stephenson, and A. R. Tajbakhsh, Phys. Rev. Lett. **57**, 98 (1986).
[13] J. D. Brock, R. J. Birgeneau, J. D. Litster, and A. Aharony, Contemp. Phys. **30**, 321 (1989).
[14] D. Y. Noh, J. D. Brock, J. O. Fossom, J. P. Hill, J. Nuttall, J. D. Litster, and R. J. Birgeneau (unpublished).
[15] S. Amador, P. S. Pershan, H. Stragier, B. D. Swanson, D. J. Tweet, L. B. Sorensen, E. B.; Sirota, G. E. Ice, and A. Habenschuss, Phys. Rev. A **39**, 2703 (1989).
[16] E. B. Sirota, P. S. Pershan, S. Amador, and L. B. Sorensen, Phys. Rev. A **35**, 2283 (1987).
[17] B. D. Swanson, H. Stragier, D. J. Tweet, and L. B. Sorensen, Phys. Rev. Lett. **62**, 909 (1980).
[18] N. D. Mermin, Phys. Rev. **176**, 250 (1968).
[19] J. M. Kosterlitz and D. J. Thouless, J. Phys. C **6**, 1181 (1973).
[20] B. I. Halperin and D. R. Nelson, Phys. Rev. Lett. **41**, 121 (1978).
[21] D. R. Nelson and B. I. Halperin, Phys. Rev. B **19**, 2457 (1979).
[22] D. R. Nelson and B. I. Halperin, Phys. Rev. B **21**, 5312 (1980).
[23] S. Ostlund, J. Toner, and A. Zippelius, Ann. Phys. (N.Y.) **144**, 345 (1982).
[24] J. V. Selinger and D. R. Nelson, Phys. Rev. Lett. **61**, 416 (1988).
[25] M. Paczuski and M. Kardar, Phys. Rev. Lett. **60**, 861 (1988).
[26] A. Aharony and M. Kardar, Phys. Rev. Lett. **61**, 2855 (1988).
[27] D. J. Tweet, R. Hołyst, B. D. Swanson, H. Stragier, and L. B. Sorensen, Phys. Rev. Lett. **65**, 2157 (1990).

[28] S. Gierlotka, P. Lambooy, and W. H. de Jeu, Europhys. Lett. **12**, 341 (1990).
[29] R. Holyst, D. J. Tweet, and L. B. Sorensen, Phys. Rev. Lett. **65**, 2153 (1990).
[30] A. Caille, C. R. Acad. Sci. Ser. B **274**, 891 (1972).
[31] R. Holyst, Phys. Rev. A **42**, 7511 (1990).
[32] See, for example, L. D. Landau and E. M. Lifshitz, *Statistical Physics* (Pergamon, Oxford, 1980), Pt. 1, p. 434.
[33] J. Als-Nielsen, J. D. Litster, R. J. Birgeneau, M. Kaplan, C. R. Safinya, A. Lindegaard-Andersen, and S. Mathiesen, Phys. Rev. B **22**, 312 (1980).
[34] P. G. de Gennes, J. Phys. (Paris) Colloq. **30**, C4-65 (1969); *The Physics of Liquid Crystals* (Oxford Univeristy Press, London, 1974), p. 288.
[35] G. Grinstein and R. A. Pelcovits, Phys. Rev. A **26**, 915 (1982).
[36] L. Gunther, Y. Imry, and J. Lajzerowicz, Phys. Rev. A **22**, 1733 (1980).
[37] K. K. Chan, M. Deutsch, B. M. Ocko, P. S. Pershan, and L. B. Sorensen, Phys. Rev. Lett. **54**, 920 (1985).
[38] C. R. Safinya, D. Roux, G. S. Smith, S. K. Sinha, P. Dimon, N. A. Clark, and A. M. Belocq, Phys. Rev. Lett. **57**, 2718 (1986).
[39] D. Roux and C. R. Safinya, J. Phys. (Paris) **49**, 307 (1988).
[40] See, for example, F. Langouche, D. Roekaerts, and E. Tirapegui, *Functional Integration and Semiclassical Expansions* (Reidel, Dordrecht, Boston, 1982), p. 10.
[41] J. D. Jackson, *Classical Electrodynamics,* 2nd ed. (Wiley, New York, 1975), p. 681.
[42] G. V. Vani and K. Vijayan, Mol. Cryst. Liq. Cryst **42**, 249 (1977).
[43] A. J. Leadbetter and M. A. Mazid, Mol. Cryst. Liq. Cryst. **65**, 265 (1981).
[44] E. F. Gramsbergen, W. H. de Jeu, and J. Als-Nielsen, J. Phys. (Paris) **47**, 711 (1986).
[45] D. J. Tweet, R. Holyst, B. D. Swanson, H. Stragier, and L. B. Sorensen (unpublished).
[46] J. V. Selinger, J. Phys. (Paris) **49**, 1387 (1988).
[47] For the dependence of the surface tension on the density difference between two coexisting phases see, for example, J. S. Rowlinson and B. Widom, *Molecular Theory of Capillarity* (Clarendon, Oxford, 1982), p. 6.
[48] B. V. Derjaguin and N. V. Churaev, J. Colloid Interface Sci. **49**, 249 (1974).
[49] B. V. Derjaguin and N. V. Churaev, J. Colloid Interface Sci. **54**, 157 (1976).
[50] A. Poniewierski and T. Sluckin, Liq. Cryst. **2**, 281 (1987).
[51] R. Evans, U. M. B. Marconi, and P. Tarazona, J. Chem. Phys. **84**, 2376 (1986).
[52] P. Kékicheff and H. K. Christenson, Phys. Rev. Lett. **63**, 2823 (1989).
[53] For the Debye-Waller factor see, for example, N. W. Ashcroft and N. D. Mermin, *Solid State Physics* (Holt, Rinehart and Winston, New York, 1976), p. 794.
[54] X. Wen and R. B. Meyer, Phys. Rev. Lett. **59**, 1325 (1987).
[55] B. Mulder, Phys. Rev. A **35**, 3095 (1987).
[56] J. V. Selinger and D. R. Nelson, Phys. Rev. A **37**, 1736 (1988).
[57] A. Poniewierski and R. Holyst, Phys. Rev. Lett. **61**, 2461 (1988); Phys. Rev. A **41**, 6871 (1990).
[58] R. Holyst and A. Poniewierski, Phys. Rev. A **39**, 2742 (1989); Mol. Phys. **71**, 561 (1990).
[59] A. M. Somoza and P. Tarazona, Phys. Rev. Lett. **61**, 2566 (1988); Phys. Rev. A **40**, 4161 (1989).
[60] L. Mederos and D. E. Sullivan, Phys. Rev. A **39**, 854 (1989).
[61] A. J. Leadbetter, M. A. Mazid, and R. M. Richardson, in *Liquid Crystals,* edited by S. Chandrasekhar (Heyden, London, 1980), p. 65.
[62] H. Lowen, T. Beier, and H. Wagner, Europhys. Lett. **19**, 791 (1989); Z. Phys. B **79**, 109 (1990).
[63] D. M. Zhu and J. G. Dash, Phys. Rev. Lett. **57**, 2959 (1986); **60**, 432 (1988).
[64] G. Gompper and D. M. Kroll, Phys. Rev. B **40**, 7221 (1989).
[65] J. F. van der Veen and J. W. M. Frenken, Surf. Sci. **178**, 382 (1986); J. W. M. Frenken and J. F. van der Veen, Phys. Rev. Lett. **54**, 134 (1985).
[66] J. Daeges, H. Gleiter, and J. H. Perepezko, Phys. Lett. **119**, 79 (1986).
[67] L. Grabaek, J. Bohr, E. Johnson, A. Johansen, L. Sarholt-Kristensen, and H. N. Andersen, Phys. Rev. Lett. **64**, 934 (1990).
[68] F. A. Lindemann, Physik A **14**, 609 (1910).
[69] F. S. Crawford, Jr., *Waves,* Berkeley Physics Course Vol. 3 (McGraw-Hill, New York, 1968), p. 429.
[70] M. Born and E. Wolf, *Principles of Optics* (Pergamon, Oxford, 1970), p. 508.
[71] H. Stragier and L. B. Sorensen (unpublished).
[72] D. J. Tweet and L. B. Sorensen (unpublished).
[73] *Statistical Mechanics of Membranes and Surfaces,* Proceedings of the 5th Jersualem Winter School for Theoretical Physics, edited by D. R. Nelson, T. Piran, and S. Weinberg (World Scientific, Singapore, 1989).
[74] R. Holyst, Phys. Rev. A **42**, 3438 (1990).